REPORT No. 905

FULL-SCALE INVESTIGATION OF AERODYNAMIC CHARACTERISTICS OF A TYPICAL SINGLE-ROTOR HELICOPTER IN FORWARD FLIGHT

By Richard C. Dingeldein and Raymond F. Schaefer

SUMMARY

As part of the general helicopter research program being undertaken by the National Advisory Committee for Aeronautics to provide designers with fundamental rotor information, the forward-flight performance characteristics of a typical single-rotor helicopter, which is equipped with main and tail rotors, have been investigated in the Langley full-scale tunnel. The test conditions included operation at tip-speed ratios from 0.10 to 0.27 and at thrust coefficients from 0.0030 to 0.0060. Results obtained with the production rotor were compared with those for an alternate set of blades having closer rib spacing and a smoother and more accurately contoured surface in order to evaluate the performance gains that are available by the use of rotor blades having an improved surface condition.

The data have been reduced in terms of the main-rotor drag-lift ratios and are presented in a series of charts which facilitate making a rapid estimation of rotor forward-flight performance. The charts may be used directly for rotors that have physical characteristics similar to either of the two test rotors. The results may be used for rotors of different solidities by applying a correction to the power drag-lift ratios used in the charts, and a chart to facilitate this correction is included.

The wind-tunnel results are shown to be in fair agreement with the results of both flight tests and theoretical predictions. The data indicate that large savings in the power required for flight at any thrust coefficient result from the use of the smooth blades. Additional smaller savings are also shown to result from operation at lower rotational speeds.

INTRODUCTION

As part of a general investigation to obtain rotor characteristics for use by helicopter designers, the forward-flight characteristics of a typical helicopter, which has a single large main rotor and a small torque-compensating tail rotor, have been investigated in the Langley full-scale tunnel. Included in the investigation was the evaluation of the resultant forces on the complete helicopter and the power input to the main rotor over a range of thrust coefficients, angles of attack, and tip-speed ratios. During a preliminary investigation of the static-thrust characteristics of six sets of rotors (reference 1), the increased performance due to improved surface condition was indicated to be greater than any increase produced by camber or twist. It was decided, therefore, to investigate also the effect of surface condition on the forward-flight performance of the helicopter. This phase of the investigation was conducted with the production rotor and a set of smooth blades used in the static-thrust tests. In addition to obtaining rotor-performance information, the forward-flight investigation served also to indicate the feasibility of testing this size and type of aircraft in the Langley full-scale tunnel by affording a comparison with the results of concurrent flight tests. The force-test data were also compared with the results of calculations made using methods of existing theory.

SYMBOLS

C_T	thrust coefficient of main rotor $\left(\frac{T}{\rho(\Omega R)^2\pi R^2}\right)$
C_{L_r}	rotor lift coefficient $\left(\frac{L}{\frac{1}{2}\rho V'^2\pi R^2}\right)$
C_{m_f}	fuselage pitching-moment coefficient $\left(\frac{\text{Fuselage pitching moment}}{\frac{1}{2}\rho V^2(\pi R^2)R}\right)$
C_{L_f}	fuselage lift coefficient $\left(\frac{\text{Fuselage lift}}{\frac{1}{2}\rho V'^2\pi R^2}\right)$
C_{D_f}	fuselage drag coefficient $\left(\frac{\text{Fuselage drag}}{\frac{1}{2}\rho V'^2\pi R^2}\right)$
T	rotor thrust, pounds
Q	rotor torque, pound-feet
Ω	angular velocity of rotor, radians per second
ρ	mass density of air, slugs per cubic foot
ρ_0	mass density of air at sea level under standard conditions, 0.002378 slug per cubic foot
r	distance from center of rotation to blade element
R	rotor blade radius, feet
V	airspeed, feet per second
L	rotor lift, pounds
σ	rotor solidity $(b\bar{c}/\pi R)$
c	chord at r
$\bar{c}$	mean chord $\left(\frac{\int_0^R cr^2dr}{\int_0^R r^2dr}\right)$
b	number of blades

μ tip-speed ratio $\left(\frac{V \cos \alpha_s}{\Omega R}\right)$

α_T geometric angle of attack set in tunnel; acute angle between the center line of tunnel and a plane perpendicular to the rotor shaft, negative when tilt is forward

α_s helicopter angle of attack; acute angle between direction of air flow and a plane perpendicular to the rotor shaft, negative when tilt is forward

θ mean blade pitch angle at $0.75R$, degrees

P/L power drag-lift ratio, ratio of drag equivalent of main-rotor-shaft power absorbed at given airspeed to rotor lift $(Q\Omega/VL)$

$(D/L)_u$ useful drag-lift ratio, ratio of rotor thrust along flight path to rotor lift

$(D/L)_r$ rotor drag-lift ratio, equal to the sum of the rotor induced drag-lift ratio and the rotor profile drag-lift ratio

DESCRIPTION OF AIRCRAFT SETUP

A photograph of the helicopter mounted on the Langley full-scale-tunnel balance supports is shown as figure 1. General characteristics and pertinent dimensions of the aircraft are given in the three-view drawing of figure 2. Additional information concerning the aircraft can be found in reference 2.

Inasmuch as it was necessary to keep the helicopter trimmed in the flight conditions simulated, a direct-reading, six-component, auxiliary strain-gage balance was designed for the tests. Modifications were made to the aircraft to permit its attachment to the strain-gage beams at each support point. Two streamline steel braces were installed between the rear tunnel support head and the two forward supports to reduce longitudinal stresses in the fuselage structure.

ROTORS TESTED

Photographs and general dimensions of the test rotor blades, which are referred to as the "production blades" and the "smooth blades," are presented in figure 3. The production blades have a radius of 19 feet measured from the center of rotation, a total area (three blades) of 65.4 square feet, and a solidity of 0.060. The blades are tapered in plan form, are untwisted, and have an NACA 0012 airfoil

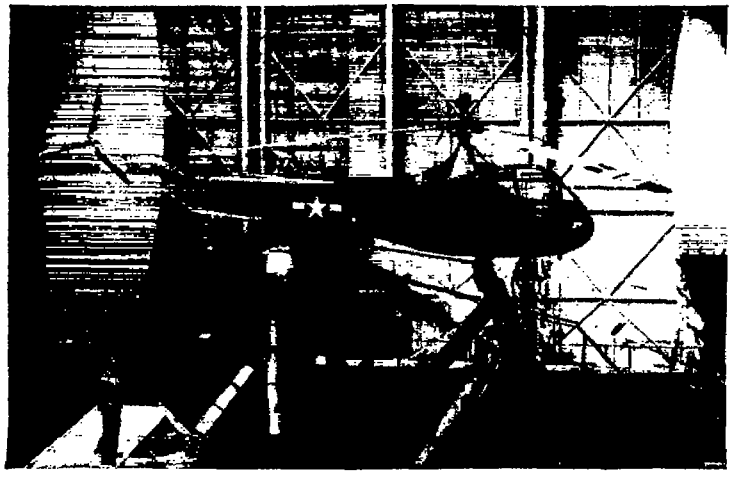

FIGURE 1.—Helicopter mounted for tests in Langley full-scale tunnel.

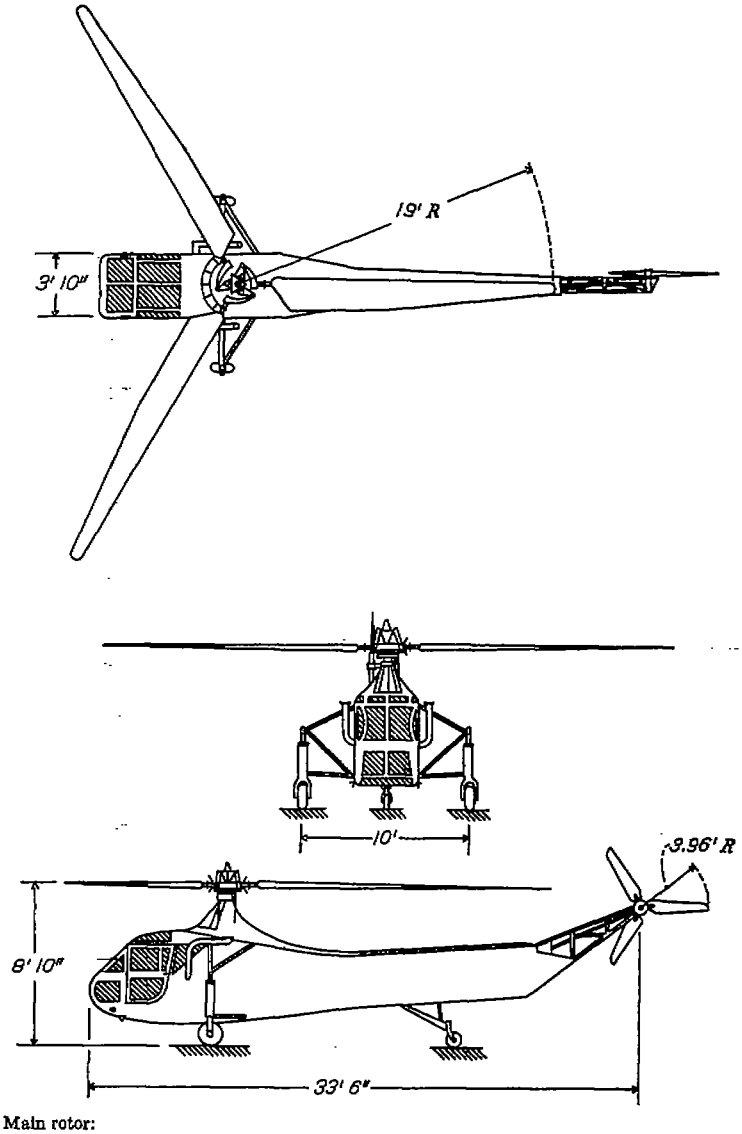

Main rotor:	
Radius, ft	19
Blade area (3 blades), sq ft	65.4
Disk area, sq ft	1134.1
Solidity	0.060
Ratio of rotational speed to engine speed	0.107
Tail rotor:	
Radius, ft	3.96
Blade area (3 blades), sq ft	4.92
Disk area, sq ft	49.2
Ratio of rotational speed to engine speed	0.567
Center line of main rotor to center line of tail rotor, ft	25.19
Parasite-drag area, sq ft	22.92
Rated horsepower	180

FIGURE 2.—Three-view drawing and pertinent dimensions of helicopter.

section. The forward 35 percent of the chord is contoured with spruce fairing strips. A wire cable forms the trailing edge, and the entire blade is covered with fabric having a standard sprayed dope finish. The smooth blades are identical to the production blades in pitch distribution, airfoil section, plan form, and solidity but have twice as many ribs outboard of the 44-percent radius. In addition, the forward 35 percent of the chord outboard of the $0.40R$ station was accurately filled to contour and given a smooth finish, and the blades were polished with wax prior to the tests.

INSTRUMENTATION

The necessary instruments, engine controls, and flight controls were operated from the test house at the rear of the

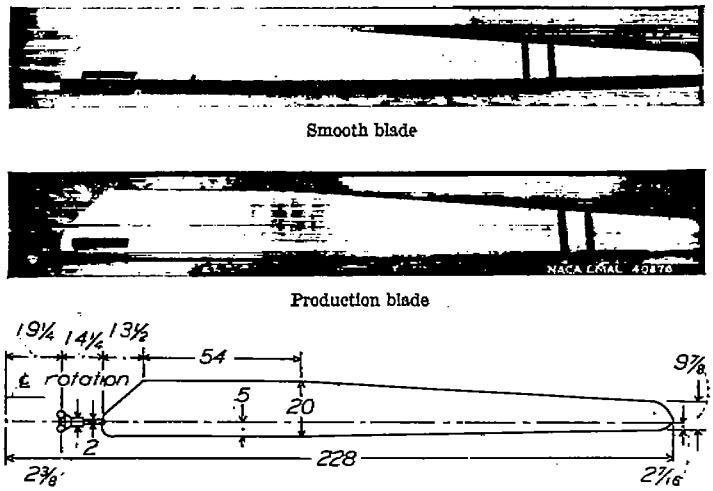

FIGURE 3.—Rotor blades tested. Lower surface shown. (All dimensions given in inches.)

balance house. (See fig. 1.) Electric actuators were used to control the cyclic feathering and tail-rotor pitch, and a hydraulic actuator operated the pitch of the main rotor. NACA control-position indicators were attached to the linkages to show the control settings. The main-rotor pitch was calibrated with a protractor fastened to one rotor blade at the 14.25-foot radius ($0.75R$) with the feathering set to zero.

In order to obtain more accurate mean blade-pitch angles than could be determined by measuring the position of the control linkages, a photographic system was used. A Bell and Howell Eyemo motor-driven 35-millimeter motion-picture camera was mounted on the crown housing aiming spanwise along one blade. Grain-of-wheat lamps were located on the upper surface of this blade near the leading and trailing edges at the $0.45R$, $0.75R$, and $0.95R$ stations. Lights on one test-chamber wall, which were photographed once during each revolution, made it possible to determine the azimuth angle for each film frame.

The shaft-power input to the main rotor and to the tail rotor was obtained by strain-gage torque meters mounted below the main-rotor thrust bearing and just forward of the tail-rotor gear box, respectively.

TESTS

Force measurements were first made to determine the aerodynamic characteristics of the fuselage for the following three configurations:

Configuration 1: Main and tail rotors removed, dummy wheels installed, and doors, windows, and cabin vents closed. This configuration is denoted as the basic condition.

Configuration 2: Same as configuration 1, except windows and cabin vents were wide open.

Configuration 3: Same as configuration 1, but with the Bell and Howell 35-millimeter motion-picture camera mounted on the crown housing. The engine was idled at 1200 rpm for this condition to average the camera tares at different azimuth angles.

Data were obtained for the three configurations at rotor-shaft angles of attack ranging from 11.5° to −15.5° for tunnel airspeeds from 30 to 85 miles per hour. Forces were measured during these tests with the standard tunnel balance system. In addition, wool tufts were mounted every 6 inches in staggered rows on the under side of the fuselage from the nose to the tail support, and the tuft behavior was observed over the same range of angles of attack at a tunnel airspeed of 62 miles per hour.

The tests with the main and the tail rotors installed were made at angles of attack (referred to tunnel axes) from 9.5° to −5.6° for tunnel airspeeds from approximately 30 to 80 miles per hour for the smooth blades. Less data were obtained for the production blades, which were expected to show inferior forward-flight performance with regard to the power required. For each run, the blade-pitch setting was varied from 4° to 12°. The side force and the rolling, pitching, and yawing moments were set at zero as indicated by the strain-gage balance. An attempt to maintain the cruising power condition at an engine speed of 2100 rpm (main-rotor speed of 225 rpm) resulted in excessive longitudinal vibration at tunnel airspeeds above 30 miles per hour. Therefore, successive reductions in engine speed to 2000, 1900, and 1800 rpm (main-rotor speed of 212, 203, and 193 rpm, respectively) were necessary as the airspeed was increased. In order to reduce vibration further, the rigidity of the supporting structure was increased by eliminating the standard tunnel balance system, making it necessary to obtain all force data from the auxiliary strain-gage balances.

During each recording of data, the motion-picture camera was operated for 2 seconds at a speed of approximately 48 frames per second.

The axes about which the moments were trimmed intersected at a point on the center line of the rotor shaft 56.52 inches below the plane of the flapping hinges. This point falls within the center-of-gravity range corresponding to normal loading.

RESULTS AND DISCUSSION

FUSELAGE

The variation of the lift, the drag, and the pitching-moment coefficients with the angle of attack for the three configurations at a tunnel airspeed of 62 miles per hour is presented in figure 4.

Opening the cabin vents and windows produced a small increase in pitching-moment coefficient, little change in lift coefficient, and had almost no effect on the fuselage-drag coefficient for forward-flight attitudes. The addition of the motion-picture camera to the basic configuration produced an even smaller increase in pitching-moment coefficient, a slight decrease in lift coefficient, and an increase in the drag coefficient of an average of 4 percent over the entire angle-of-attack range. The variation of pitching-moment coefficient with angle of attack was either neutral or unstable for all three configurations throughout the angle-of-attack range.

The horsepower required to overcome the fuselage drag at different airspeeds for the basic condition is given in figure 5. The values at airspeeds below 30 miles per hour were obtained by extrapolation and are indicated by a broken line. The fuselage angles of attack for which the power was calculated were obtained from data in reference 2. At an airspeed of 80 miles per hour, 68 horsepower or almost 38 percent of the rated power of this helicopter is

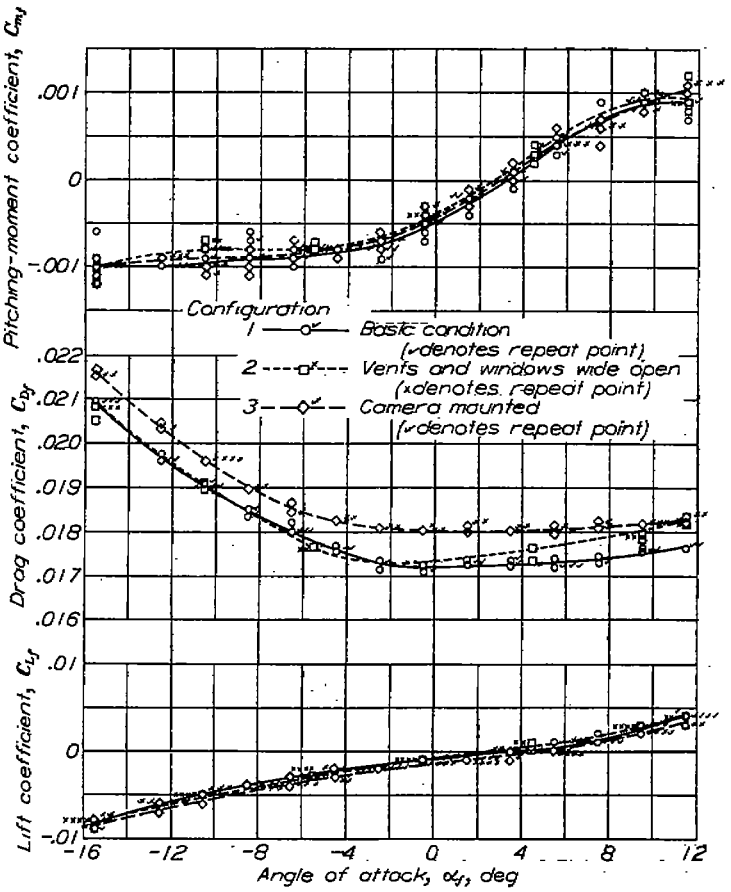

FIGURE 4.—Aerodynamic characteristics of helicopter fuselage. Main and tail rotors removed; coefficients based on main-rotor disk area of 1134 square feet; tunnel airspeed, 62 miles per hour.

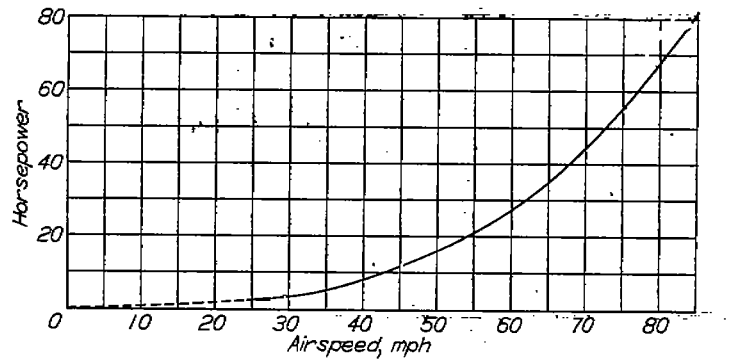

FIGURE 5.—Power required to overcome fuselage drag in trimmed flight. Fuselage configuration 1.

required to overcome the fuselage drag. For the high-speed attitude of −10° the equivalent parasite-drag area based on a coefficient of unity is 21 square feet. The minimum drag coefficient referred to the projected frontal area of the fuselage is approximately 4½ times that of a conventional airplane fuselage.

The observations of the tufts on the under side of the fuselage for angles of attack from 11.5° to −15.5° are shown in figure 6. The representation of disturbed flow shows approximately the magnitude of the tuft motion. Separated flow, indicative of large drag losses, was present behind the constant-width section of the fuselage at all negative angles of attack. This result is in agreement with the rapid increase in drag coefficient observed from the force data. (See fig. 4.)

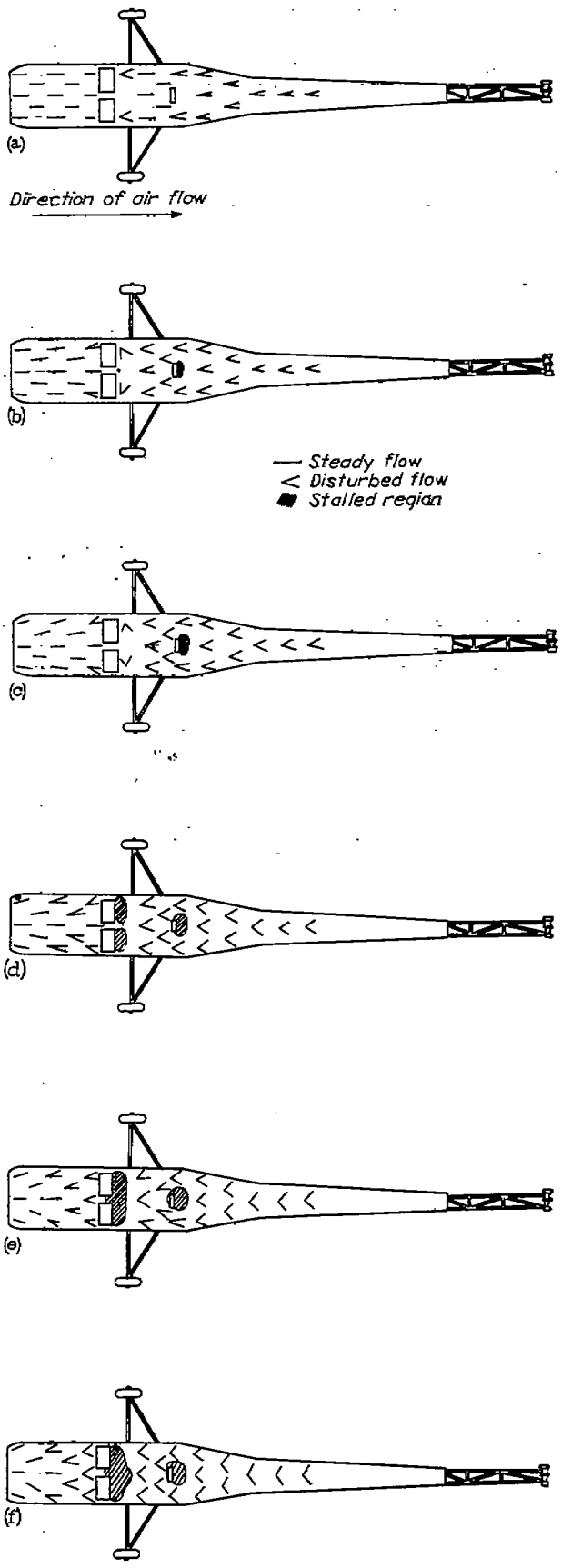

(a) α_s=11.5°.
(b) α_s=3.5°.
(c) α_s=0.5°.
(d) α_s=−6.5°.
(e) α_s=−10.5°.
(f) α_s=−15.5°.

FIGURE 6.—Tuft observations on underside of helicopter fuselage. Tunnel airspeed, 62 miles per hour.

ROTOR CHARACTERISTICS

Inasmuch as it is desirable to present the results in terms of the characteristics of the main rotor alone in order that they might be more readily adapted to general use, the fuselage, the rotor hub, and the tail rotor have been in a sense considered as supports for the main rotor. The data have accordingly been reduced by the following procedure: The helicopter angle of attack and the lift and the drag coefficients used in the calculations were corrected for the jet-boundary effect by using the usual tunnel correction for a wing having the same area and lift as the rotor disk. A plot of this jet-boundary correction as a function of rotor lift coefficient is shown in figure 7. A stream-angle correction of $-0.5°$ was also applied to the data. The rotor drag-lift ratios were evaluated from the following relationship given in reference 3:

$$\frac{P}{L}=\left(\frac{D}{L}\right)_0+\left(\frac{D}{L}\right)_i+\left(\frac{D}{L}\right)_p+\left(\frac{D}{L}\right)_c \tag{1}$$

where

P/L power drag-lift ratio, ratio of drag equivalent of main-rotor-shaft power absorbed at given airspeed to rotor lift ($Q\Omega/VL$)

$\left(\frac{D}{L}\right)_0$ rotor profile drag-lift ratio

$\left(\frac{D}{L}\right)_i$ rotor induced drag-lift ratio

$\left(\frac{D}{L}\right)_p$ parasite drag-lift ratio

$\left(\frac{D}{L}\right)_c$ ratio of force along flight path available for horizontal acceleration or climb to rotor lift

Previous experience has shown it convenient to regroup the terms of equation (1) to give the relationship

$$\frac{P}{L}=\left(\frac{D}{L}\right)_r+\left(\frac{D}{L}\right)_u \tag{2}$$

where

$\left(\frac{D}{L}\right)_r$ rotor drag-lift ratio $\left(\left(\frac{D}{L}\right)_0+\left(\frac{D}{L}\right)_i\right)$

$\left(\frac{D}{L}\right)_u$ useful drag-lift ratio, ratio of total rotor thrust along the flight path to rotor lift

$$\left(\left(\frac{D}{L}\right)_u=\left(\frac{D}{L}\right)_p+\left(\frac{D}{L}\right)_c=\left(\frac{D}{L}\right)_{p_f}+\left(\frac{D}{L}\right)_{p_t}-\left(\frac{D}{L}\right)_b\right)$$

and subscripts

p_f parasite drag of fuselage
p_t parasite drag of tail rotor
b drag measured by wind-tunnel balance

In equation (2), P/L and $(D/L)_u$ were readily obtained from readings of the torque meter and the auxiliary strain-gage balance during tests of the complete helicopter and from the results of the fuselage force tests previously discussed. The rotor lift used in each term of this equation has been corrected for the estimated downward load on the fuselage due to the induced flow through the rotor. This correction was obtained by assuming the fuselage attitude to be the aerodynamic angle of attack minus the induced downwash angle at the rotor, which was taken as $57.3C_{L_r}/4$ degrees. Inasmuch as the camera was mounted on the helicopter throughout the tests, the fuselage tares obtained for configuration 3 were used in reducing the data.

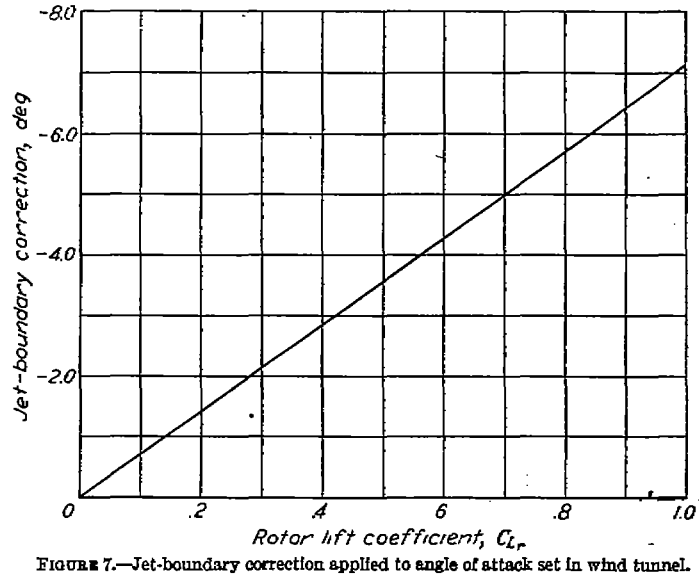

FIGURE 7.—Jet-boundary correction applied to angle of attack set in wind tunnel.

It was necessary to resort to the theory of reference 4 to estimate the parasite drag of the tail rotor. This estimate was made by determining the theoretical value of the mean section profile-drag coefficient, which corresponded to the shaft-power input obtained from the tail-rotor torque-meter reading. From this profile-drag coefficient and the value of the tail-rotor lift obtained from the measured main-rotor-shaft torque input and helicopter yawing moments, the ratio of the parasite drag to the lift of the tail rotor was calculated. The equivalent parasite-drag area of the tail rotor based on a coefficient of unity was of the order of 1 square foot for all test conditions.

The mean blade-pitch angle of the main rotor at the $0.75R$ station θ was obtained from the camera records. When records were not available, the value of θ was determined from the reading of the indicator attached to the pitch-control linkage and from a calibration curve of this indicated pitch angle plotted against the mean pitch angle taken from the camera records. The accuracy with which the mean pitch angle could be found was about $\pm 0.25°$.

The final plots presenting the results of the forward-flight investigation were derived as follows:

(1) Values of P/L, $(D/L)_u$, C_{L_r}, and α_s were plotted against tip-speed ratio μ for the values of mean pitch angle θ at which the tests were made. These curves were prepared for each tunnel angle of attack α_T. A faired plot of the data obtained at a tunnel angle of attack of $-5.6°$ is shown as a sample in figure 8. It should be noted that the corrected angle of attack α_s differs from α_T by the magnitude of the jet boundary and stream-angle corrections. The symbol α_s defines the attitude of the rotor shaft with respect to the free-stream direction but does not represent the forward tilt of the axis of zero feathering, which differs from α_s by the longitudinal feathering required for trim.

(2) Cross plots of the curves in item 1 were made in which P/L, $(D/L)_u$, C_{L_r}, and α_s were plotted against θ for a range of values of μ. A sample cross plot at $\alpha_T=-5.6°$ is shown in figure 9. The curves drawn in this figure pass through each of the cross-plotted points taken from the data plotted in step 1 and are not faired again.

(3) At even values of θ, the terms P/L, $(D/L)_u$, and C_{L_r} were next plotted against α_s for a range of values of μ. These plots eliminated α_T as a variable. A sample cross plot made for a pitch angle of 8° is presented in figure 10. As in the previous step, the curves pass through each of the cross-plotted points.

(4) Finally, C_{L_r} and $(D/L)_u$ were plotted against P/L for conditions of constant mean blade pitch angle and for conditions of constant rotor-shaft tilt (fig. 11). Plots were made for each tip-speed ratio. In this final step any small waviness in the curves were faired out. The lift coefficients corresponding to values of rotor thrust coefficient of 0.0030, 0.0040, 0.0050, and 0.0060 were then calculated for each chart from the relationship

$$C_L=\frac{2C_T}{\mu^2}\cos^3\alpha_s$$

with a value of unity assumed for the term $\cos^3\alpha_s$. The lines of constant-thrust coefficient were then drawn on the plots of C_{L_r} against P/L and of $(D/L)_u$ against P/L to the extent of the data. Although excessive vibration necessitated progressive reductions in the rotor speed as the tunnel airspeed was increased, the data obtained at the different rotor speeds are in good agreement. Sufficient overlapping of test data is present to indicate that any effects due to operating the rotor at different speeds are within the experimental accuracy.

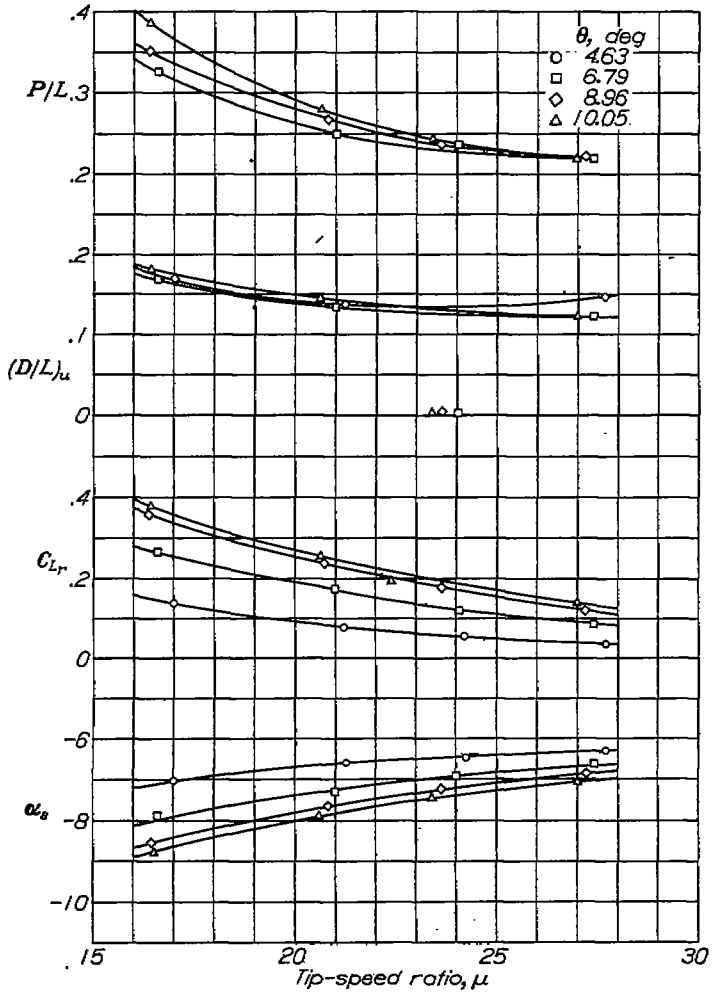

FIGURE 8.—Initial plot of main-rotor parameters. $\alpha_T=-5.6°$.

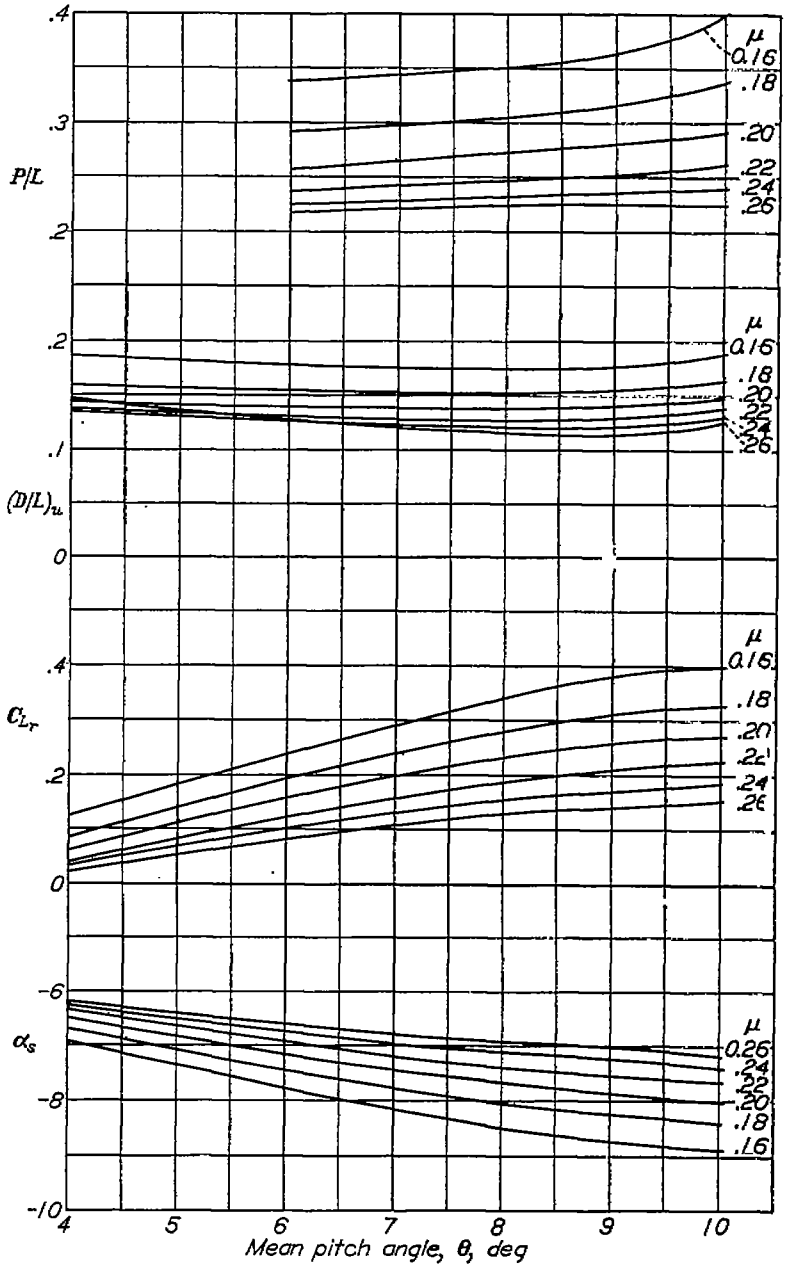

FIGURE 9.—First cross plot of main-rotor parameters. $\alpha_T=-5.6°$.

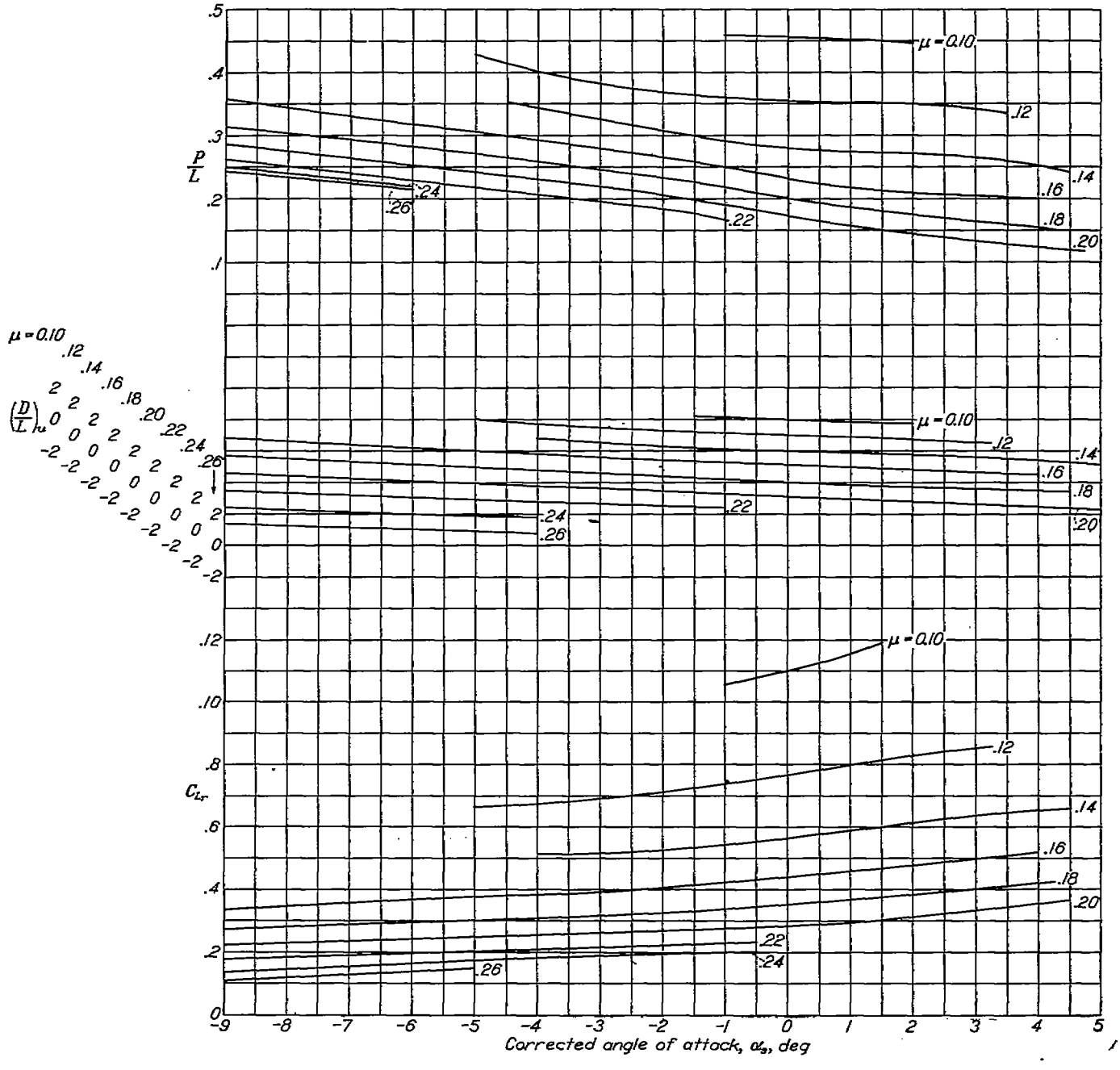

FIGURE 10.—Sample of second series of cross plots of main-rotor parameters $\theta = 8°$.

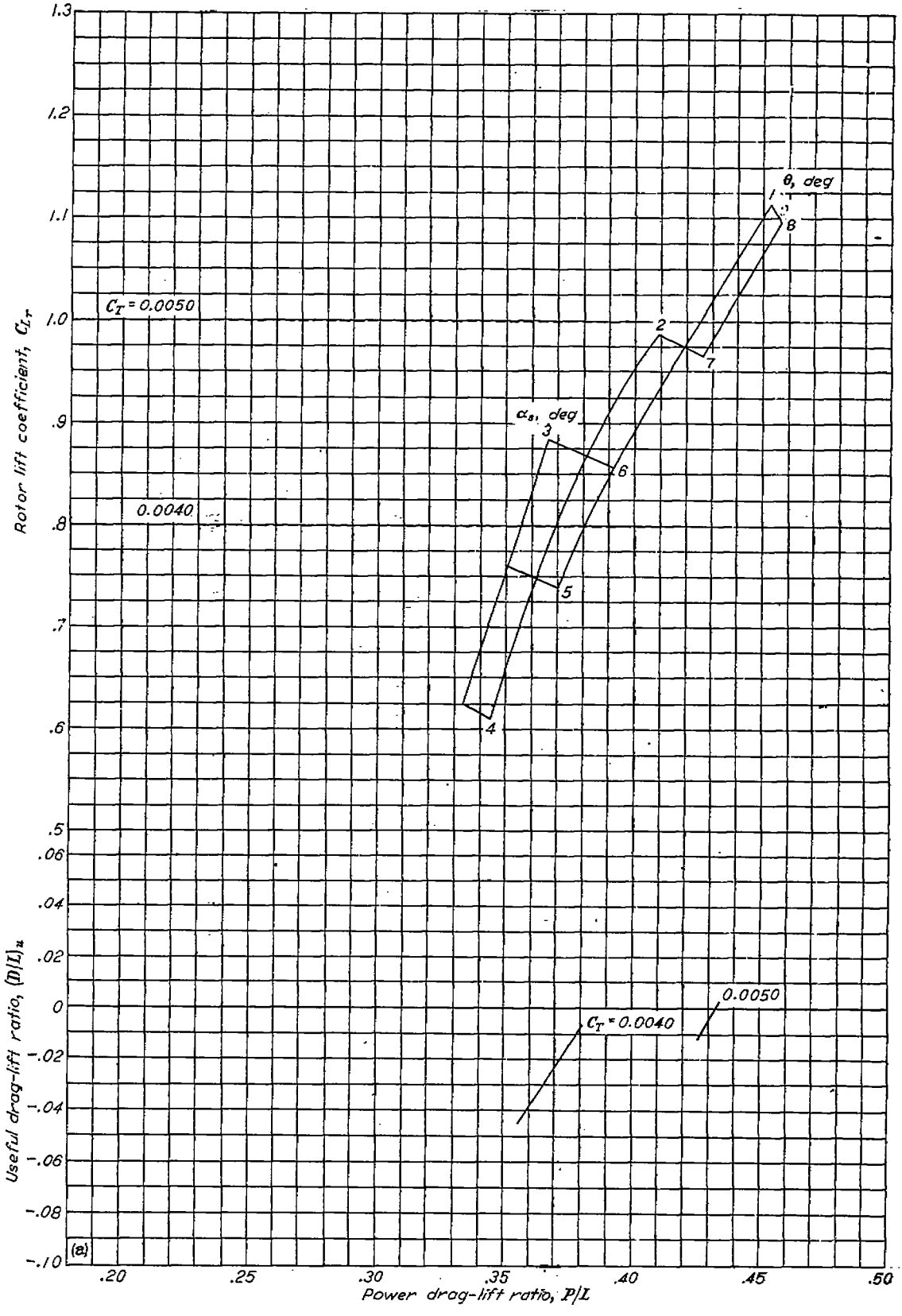

(a) μ=0.10.

FIGURE 11.—Aerodynamic characteristics of the smooth rotor.

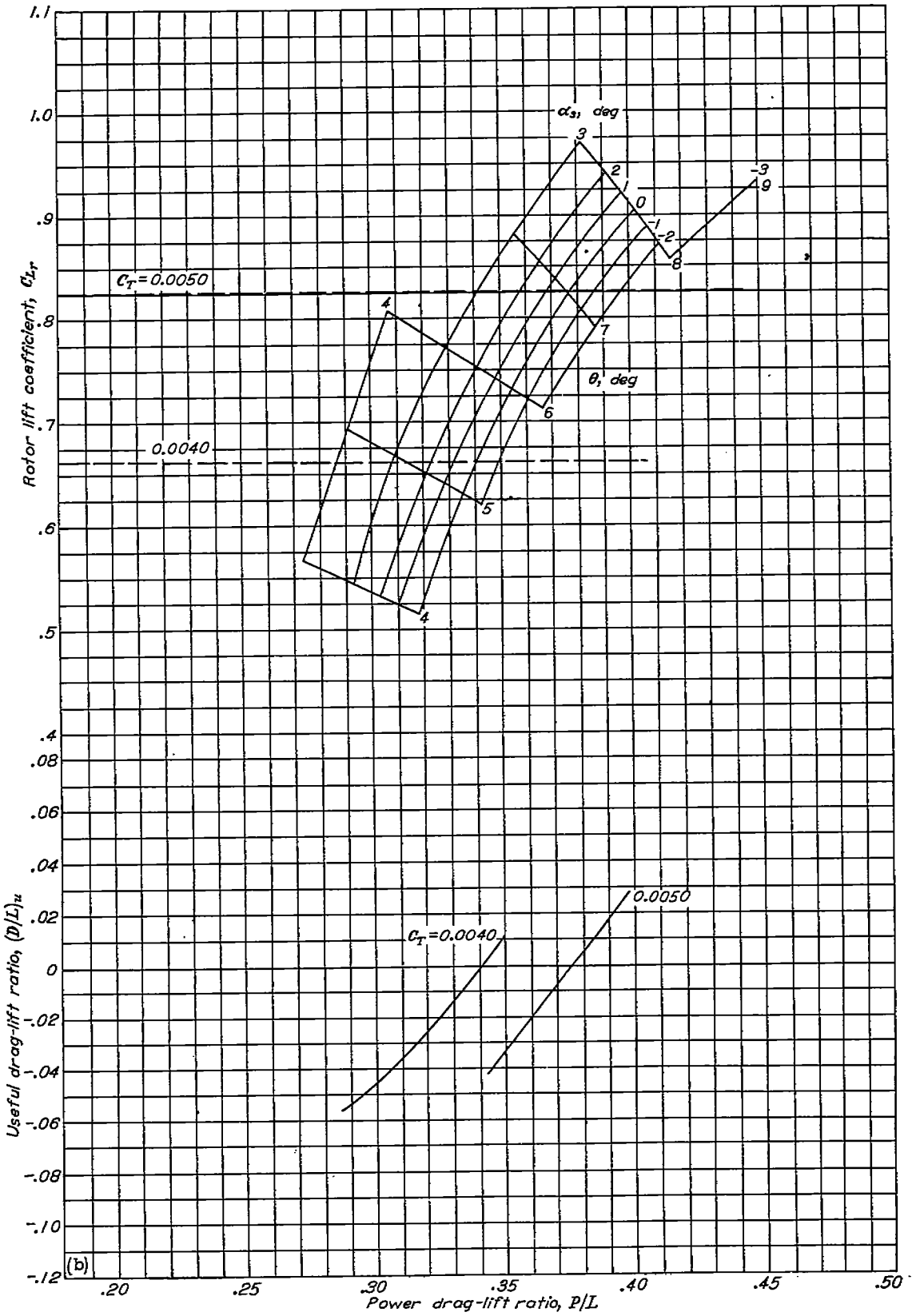

(b) μ=0.11.

FIGURE 11.—Continued.

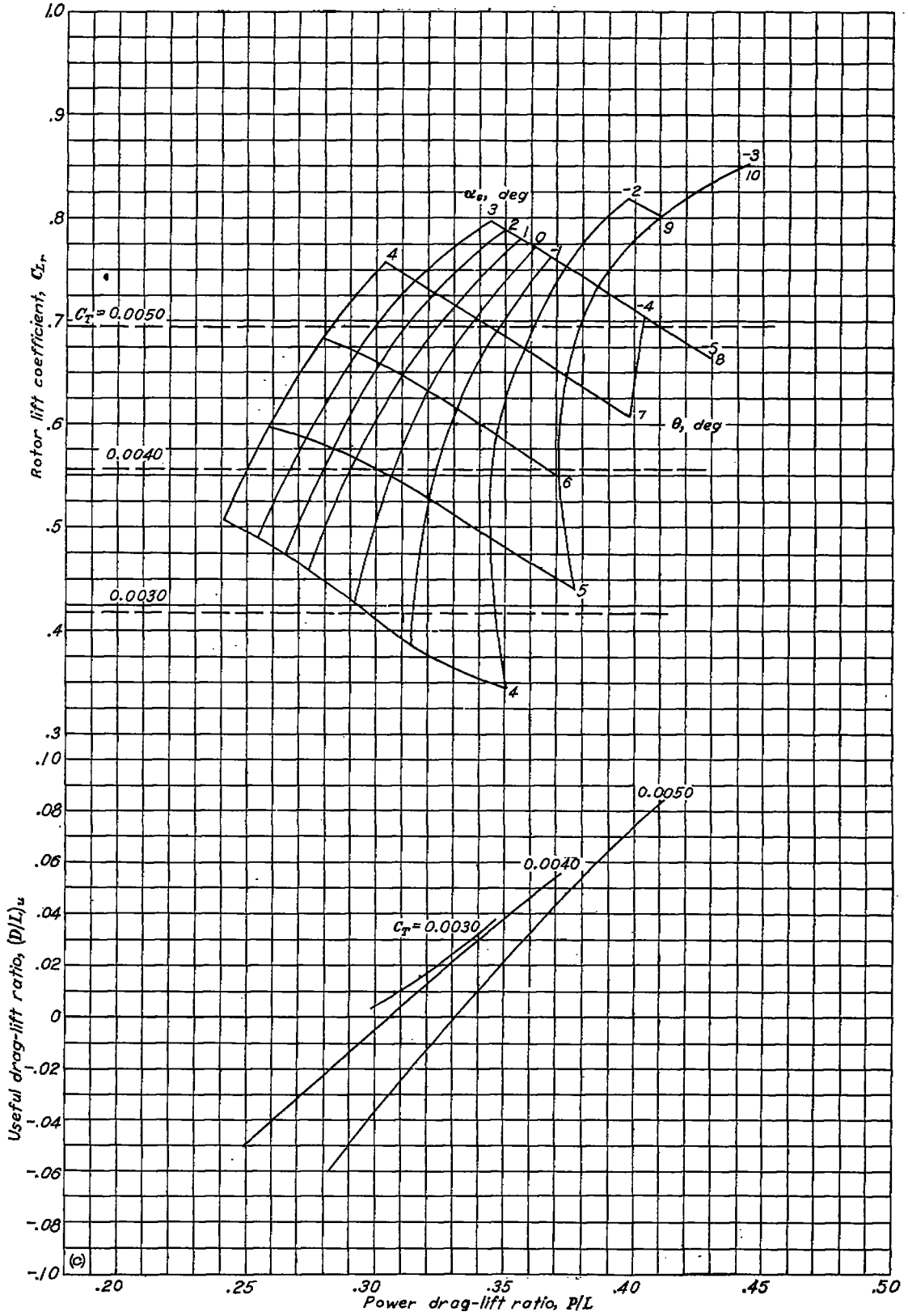

(c) $\mu = 0.12$.

FIGURE 11.—Continued.

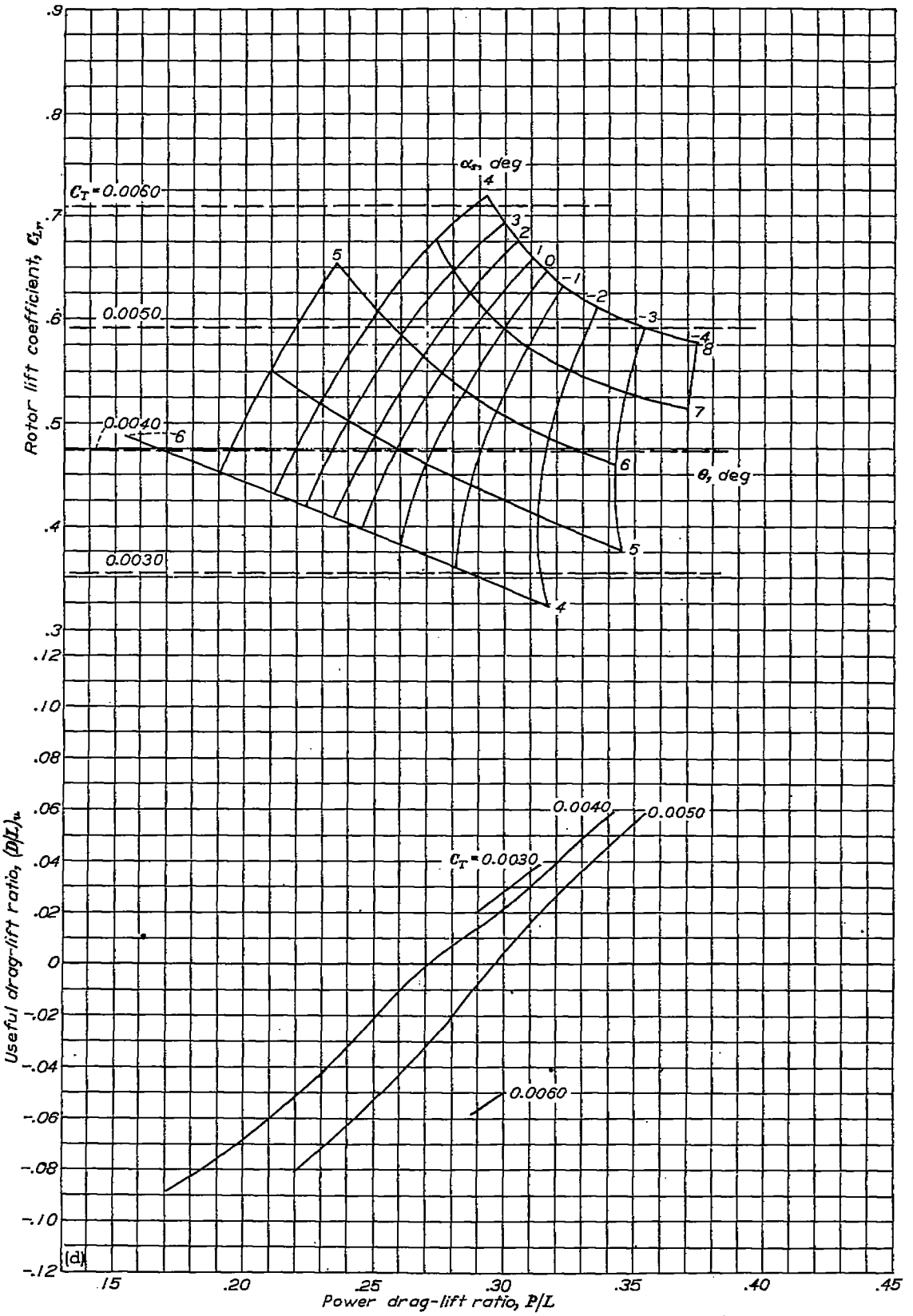

(d) μ=0.13.

FIGURE 11.—Continued.

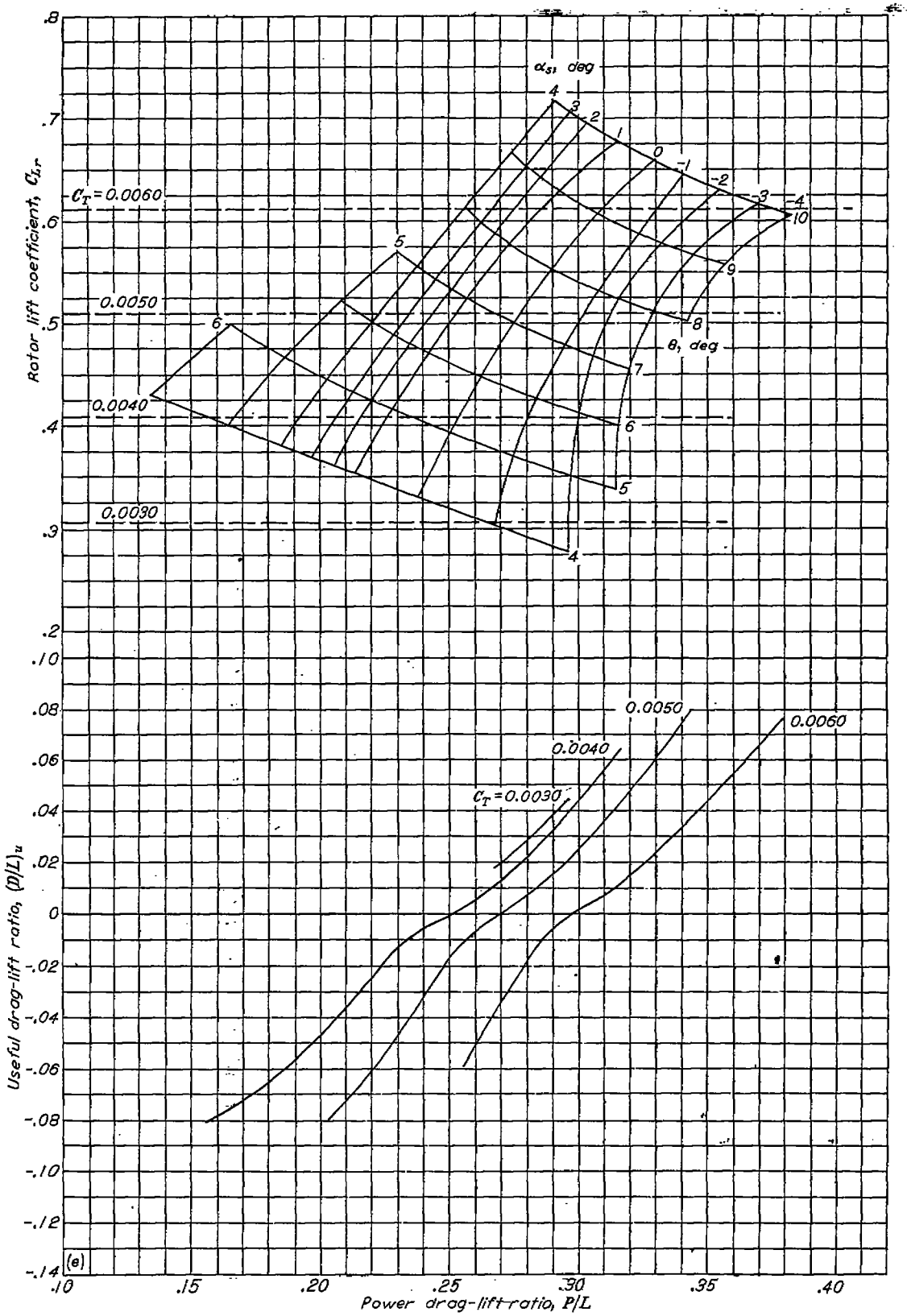

(e) μ=0.14.

FIGURE 11.—Continued.

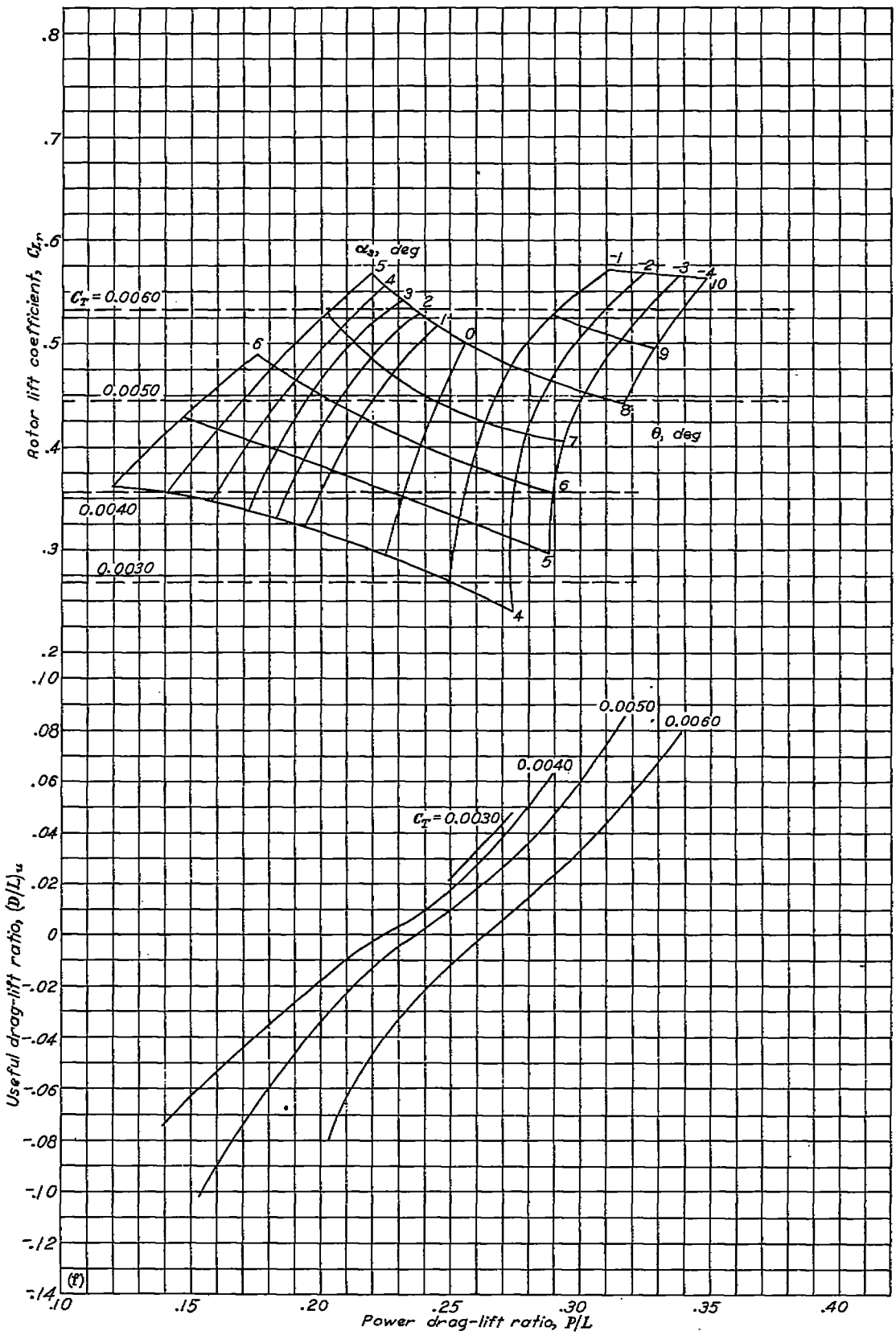

(f) μ=0.15.

FIGURE 11.—Continued.

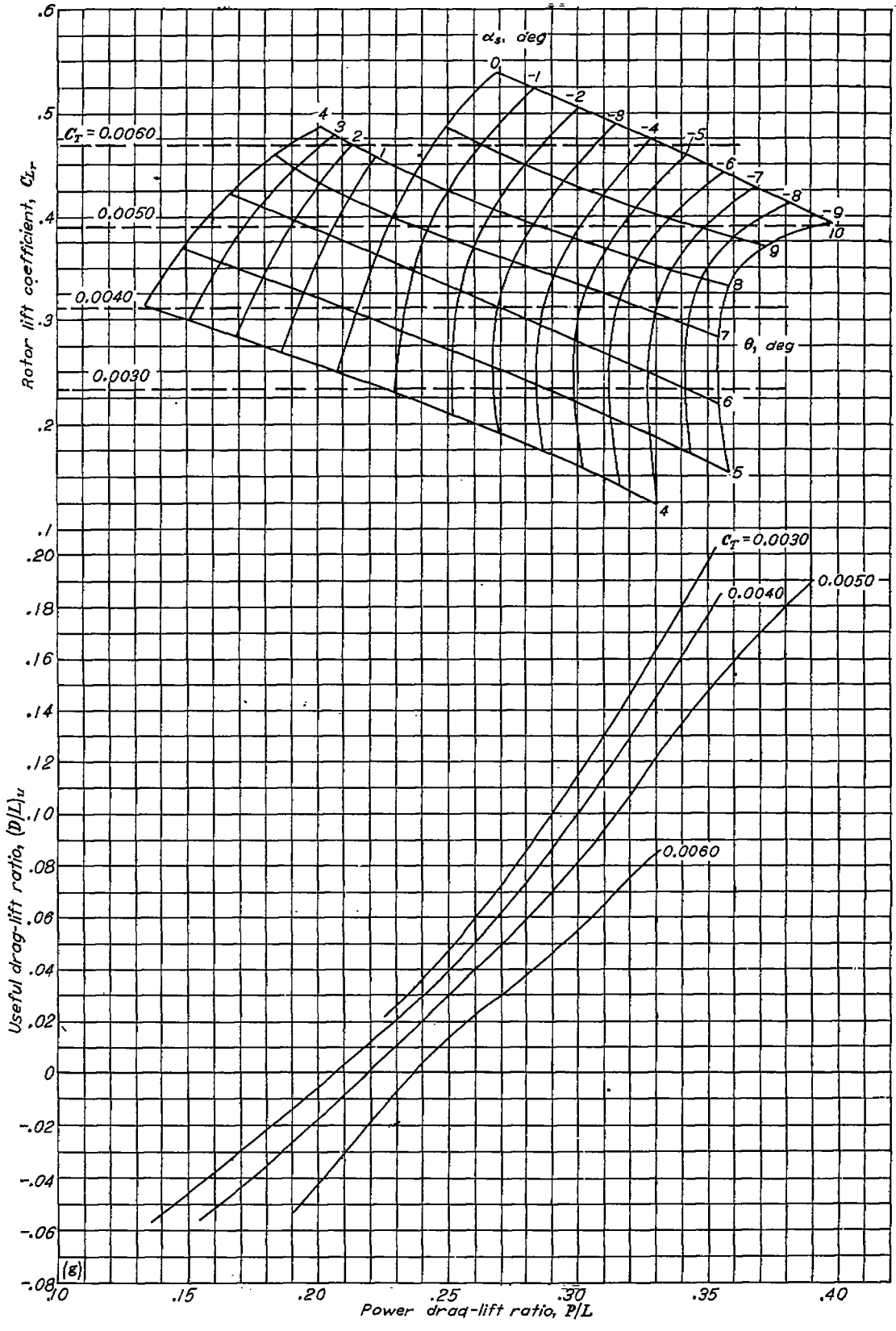

(g) $\mu = 0.16$.

FIGURE 11.—Continued.

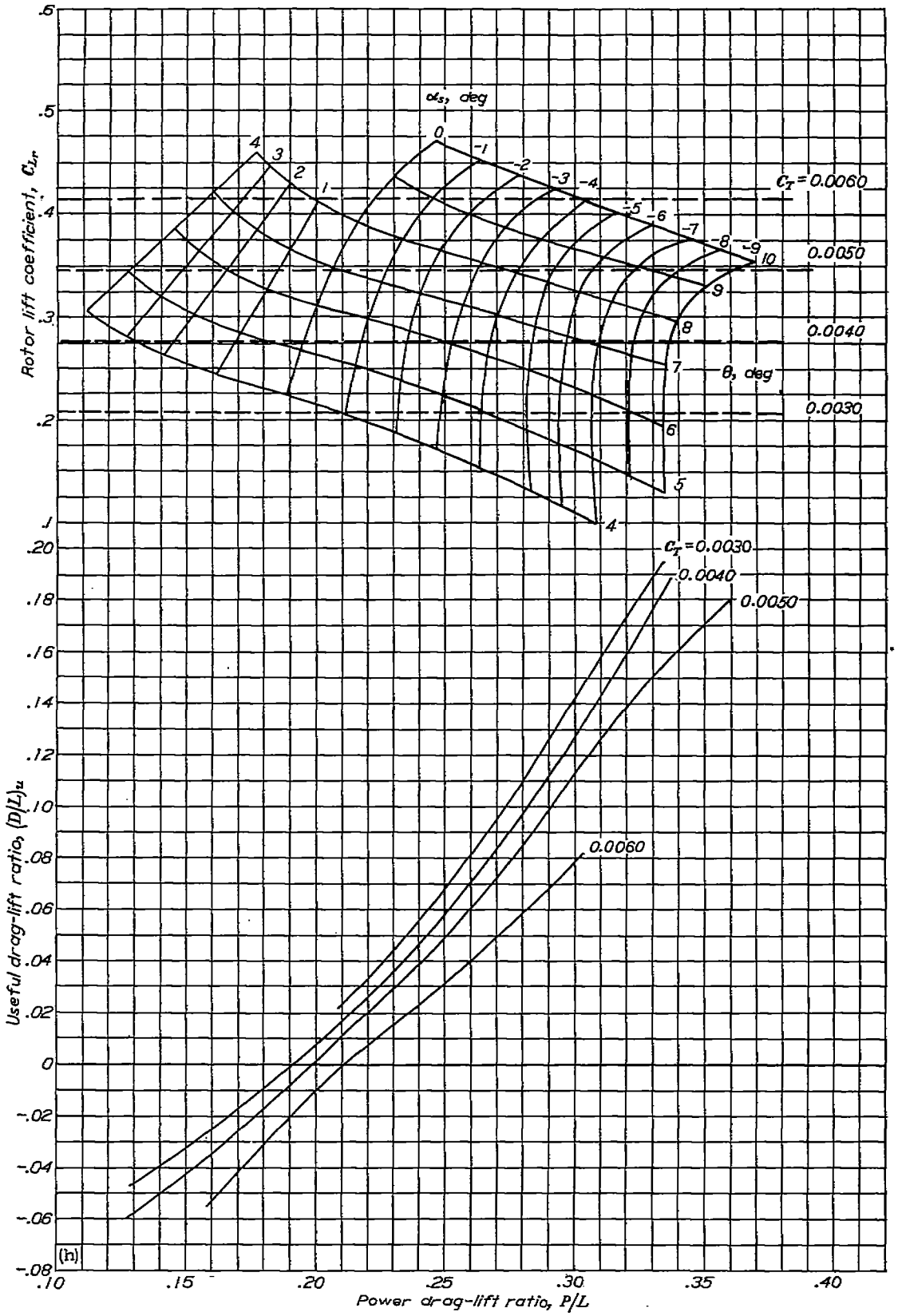

(h) μ=0.17.

FIGURE 11.—Continued.

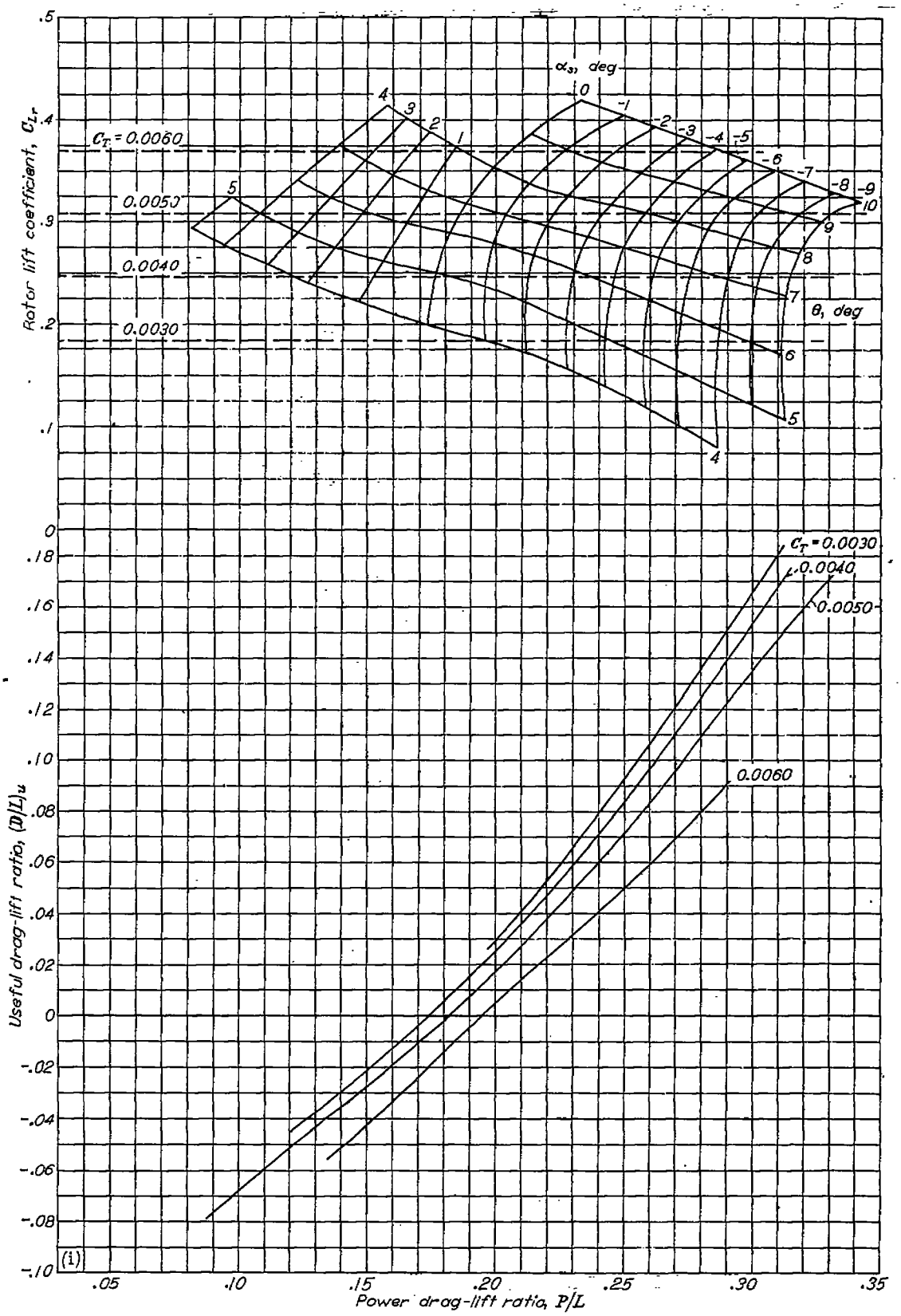

(i) μ=0.18.

FIGURE 11.—Continued.

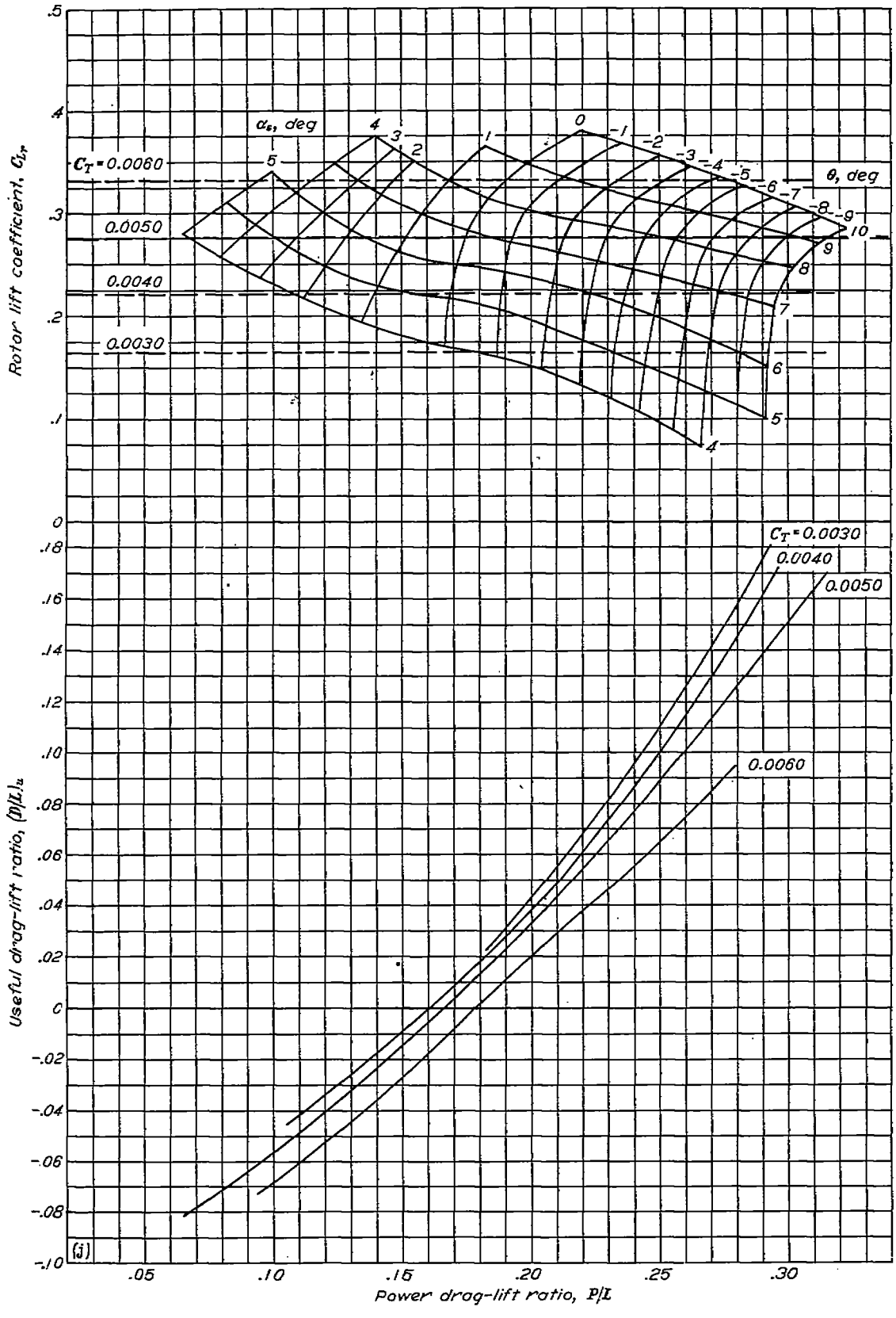

(j) μ=0.19.

FIGURE 11.—Continued.

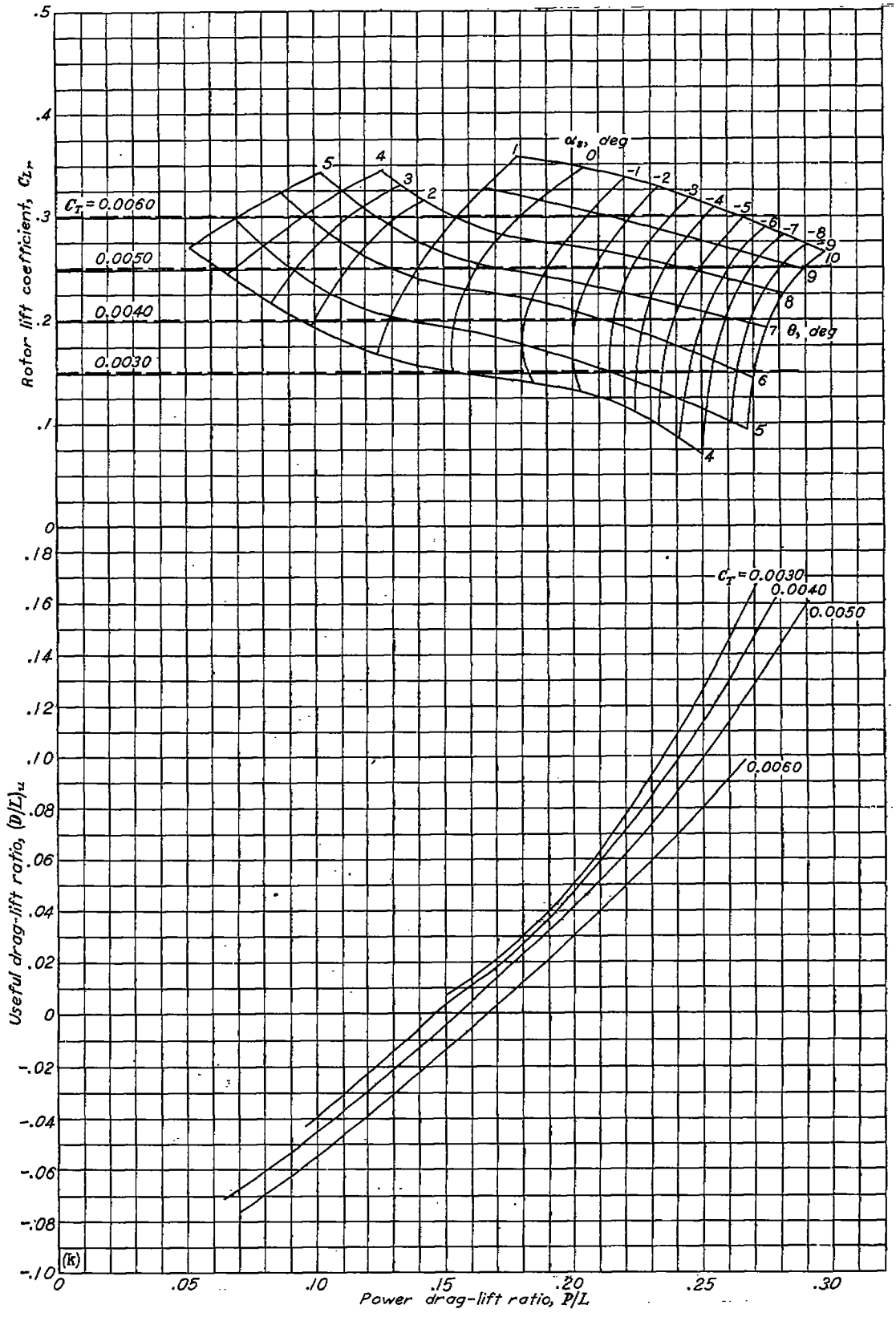

(k) μ=0.20.

FIGURE 11.—Continued.

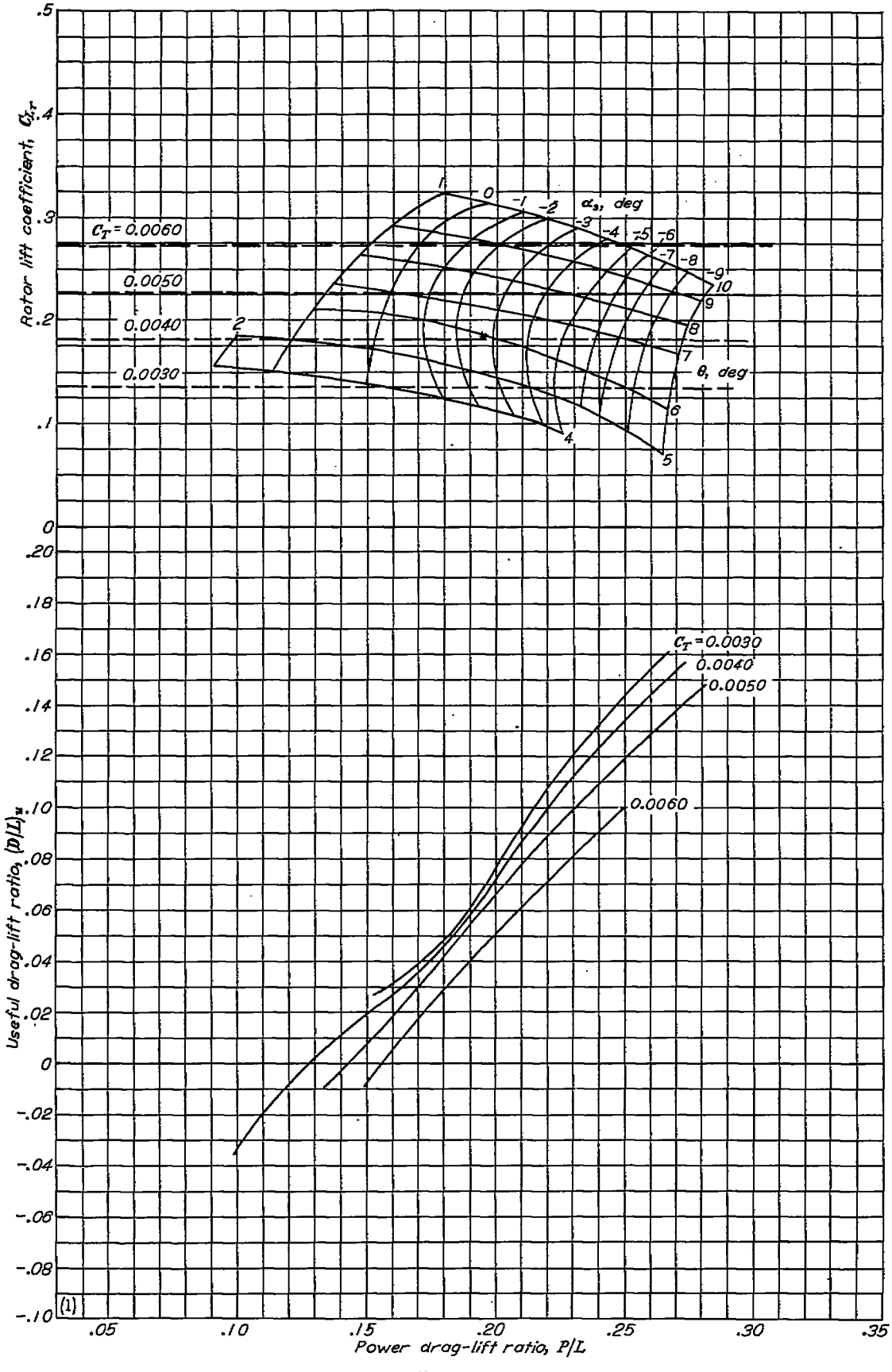

(1) μ=0.21.

FIGURE 11.—Continued.

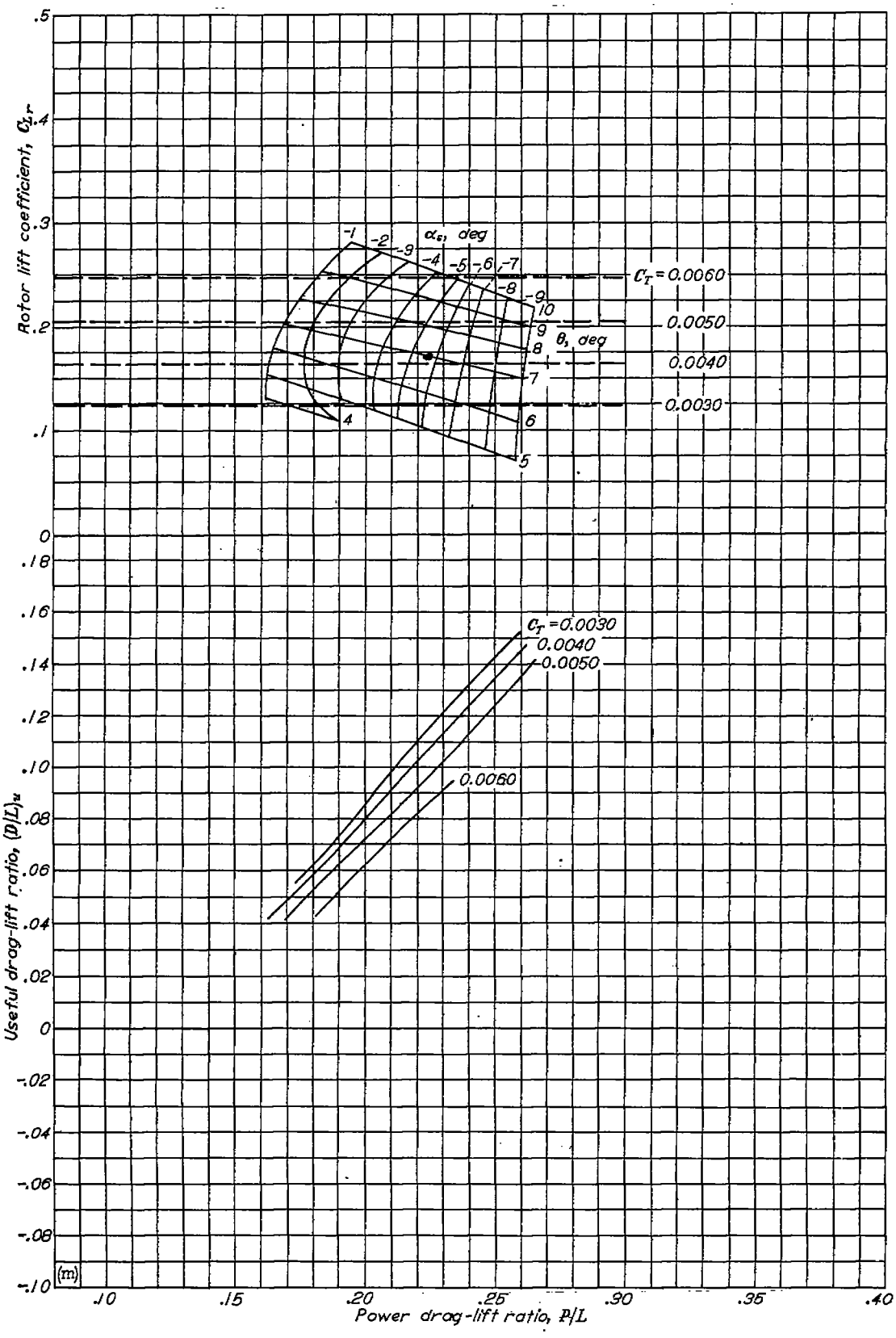

(m) μ=0.22.

FIGURE 11.—Continued.

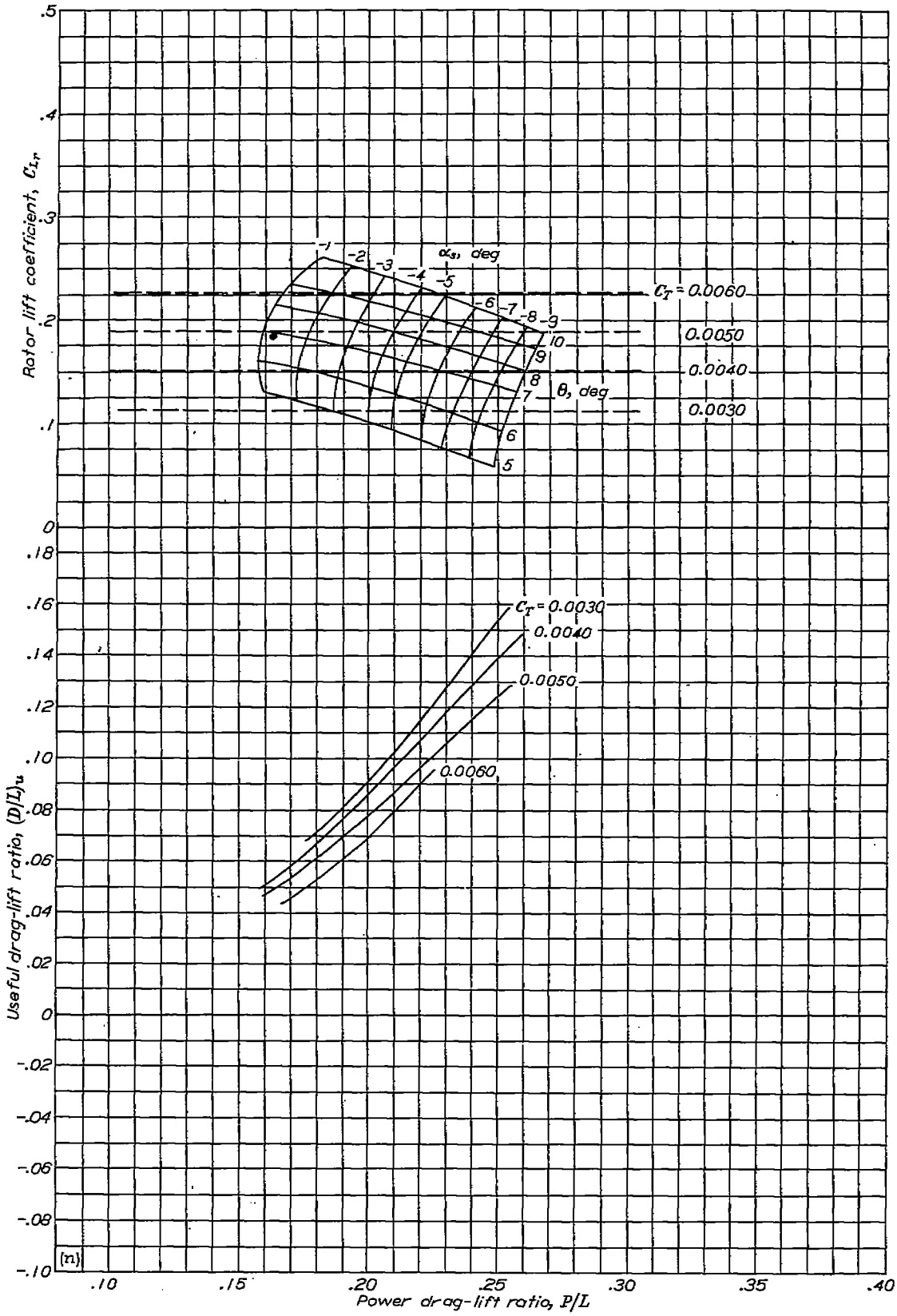

(n) μ=0.23.

FIGURE 11.—Continued.

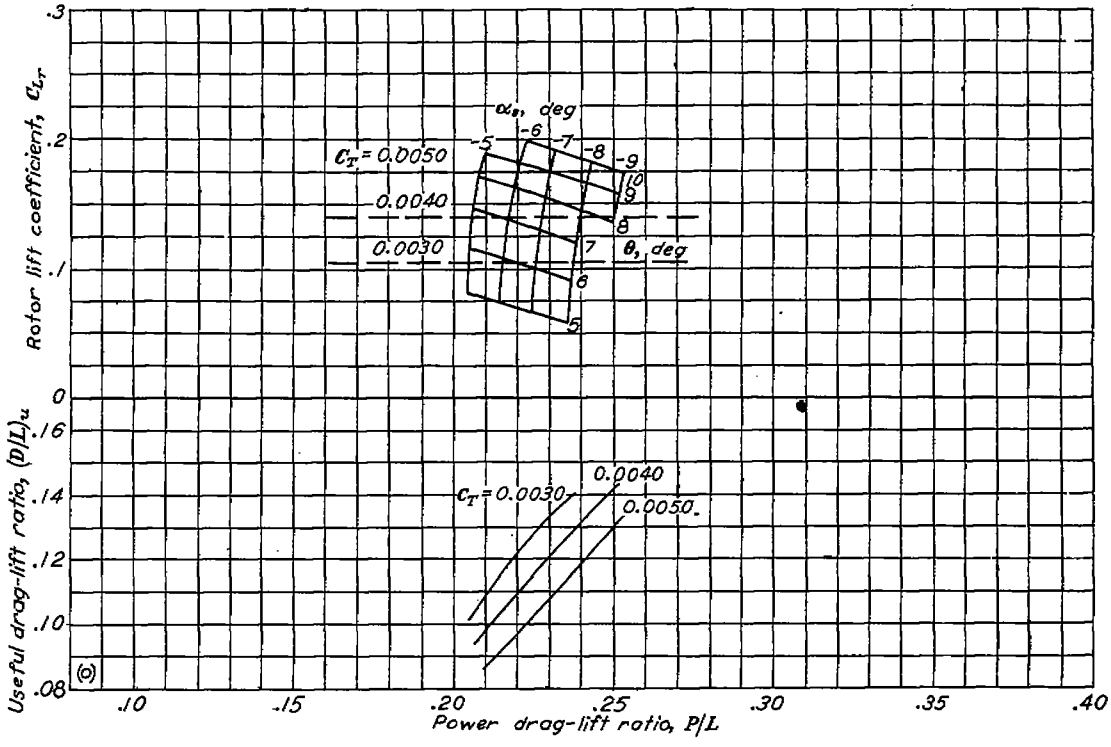

(o) μ=0.24.

FIGURE 11.—Continued.

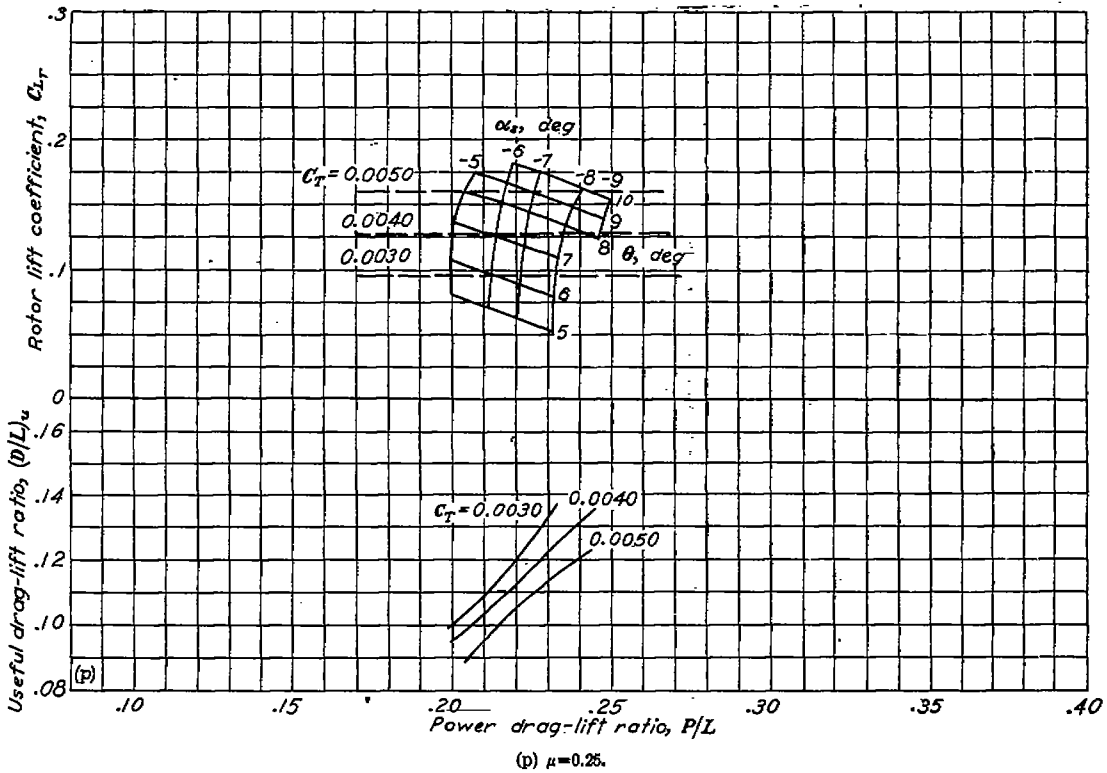

(p) μ=0.25.

FIGURE 11.—Continued.

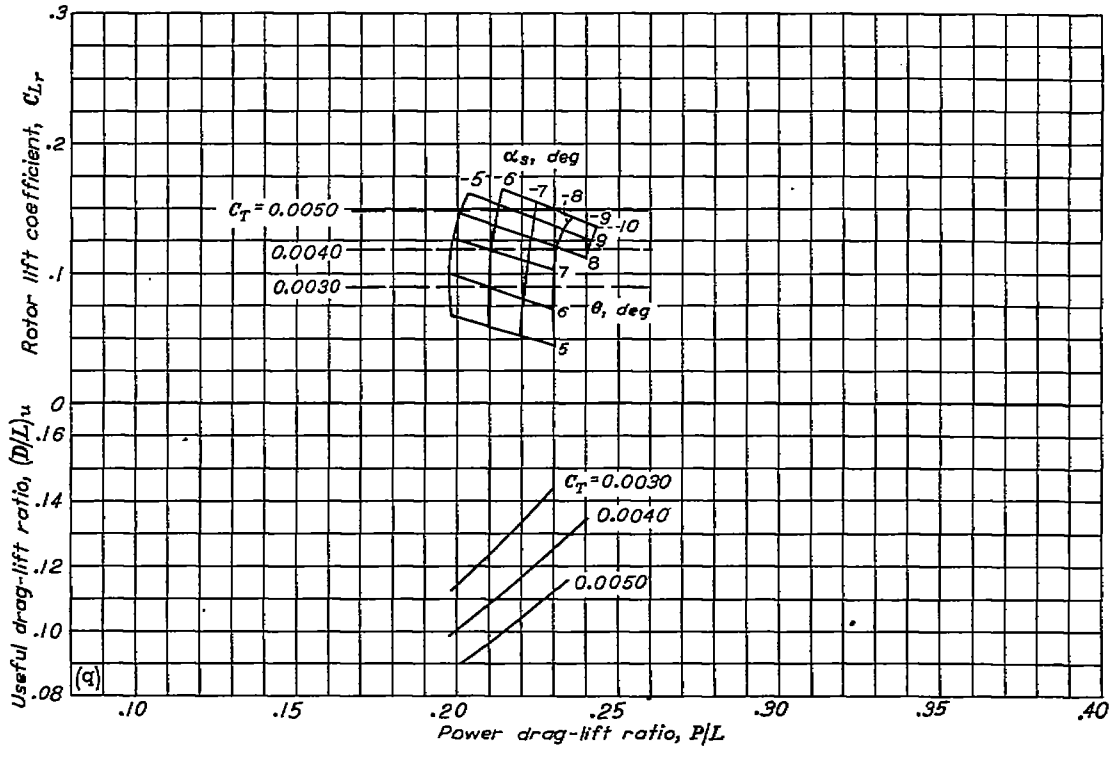

(q) μ=0.26.

FIGURE 11.—Continued.

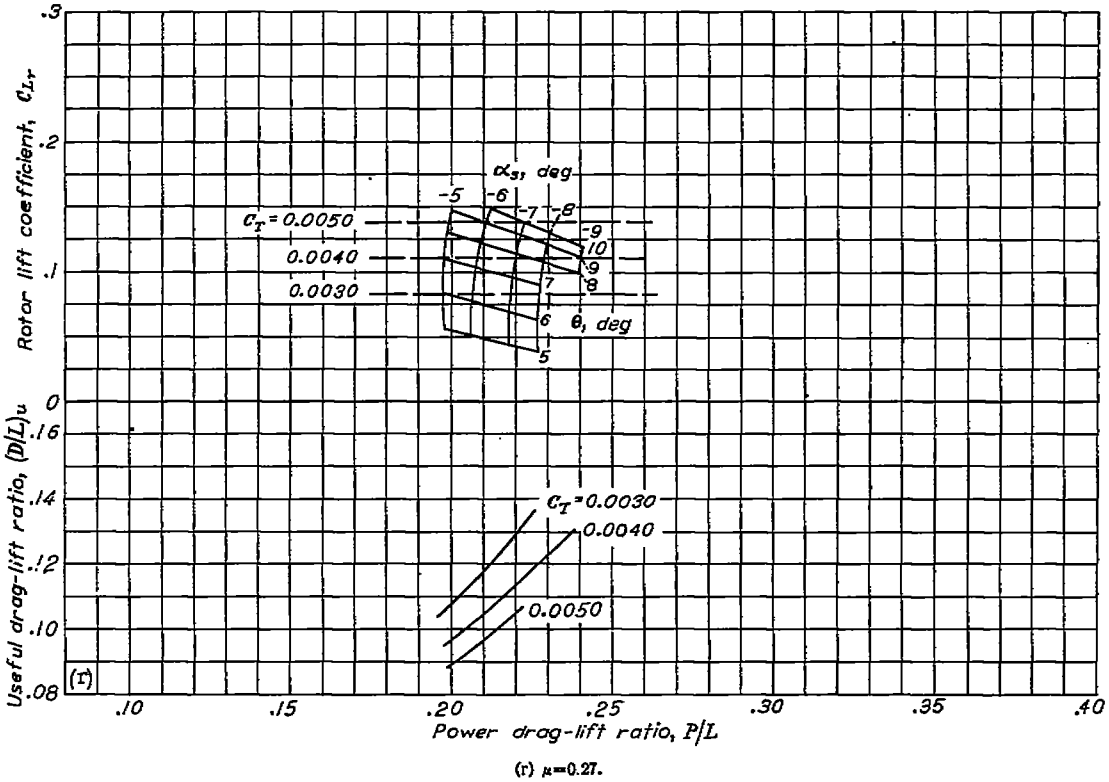

(r) μ=0.27.

FIGURE 11.—Concluded.

Charts of this form are presented for the smooth blades in figure 11 for tip-speed ratios from 0.10 to 0.27. Similar charts prepared from the data obtained for the production blades are given in figure 12 for tip-speed ratios from 0.17 to 0.22. The lines of constant mean blade-pitch angle and rotor-shaft angle of attack have been omitted from the lower part of the charts for clarity.

These data, which were obtained on a rotor of 0.06 solidity, may conveniently be applied to the study of rotors of other solidities by making a correction to the power drag-lift ratios. This correction represents the calculated change in rotor induced drag-lift ratio caused by a change in solidity at a fixed blade loading C_T/σ. From the simplifying assumption (reference 4) that the rotor induced drag-lift ratio is equivalent to $C_{L_r}/4$, the corrections to be applied to the values of power drag-lift ratio obtained from the charts of figures 11 and 12 have been calculated for solidities of 0.03 and 0.09. The corrections are presented in figure 13 as a function of tip-speed ratio for values of C_T/σ of 0.05 and 0.10. A linear interpolation may be used in obtaining the corrections for other values of σ and C_T/σ. As the simplified method of computing the rotor induced drag-lift ratios is accurate only for a tip-speed ratio of 0.15 or higher, the corrections are not included for the lower tip-speed ratios.

The power required for a helicopter in steady flight over a range of thrust coefficients and tip-speed ratios and equipped with either of two rotors tested can be easily determined from the charts, provided that the fuselage characteristics for different airspeeds are known or can be estimated. From the charts just presented, the fuselage data for the basic configuration (fig. 4) corrected for the effect of the rotor-induced velocities, together with the variation of the helicopter angle of attack with airspeed from the data of reference 2, and the one-square-foot parasite-drag area of the tail rotor previously determined, the horsepower required for the helicopter in unaccelerated horizontal flight at different airspeeds was computed. The calculations were made at thrust coefficients of 0.0050 and 0.0060 for the helicopter having the smooth blades and at a thrust coefficient of 0.0060 for the same helicopter having the production blades. At a few tip-speed ratios a small extrapolation of the lines of constant thrust coefficient shown in figures 11 and 12 was made. The results are shown in figure 14. As flight data obtained at a gross weight of 2,560 pounds and a density ratio of 0.924 were available from reference 2 for the production blades, all calculations were based on this weight and density to permit a comparison of the tunnel results with those of the flight tests. The flight-test data for $C_T=0.0060$ are included in figure 14.

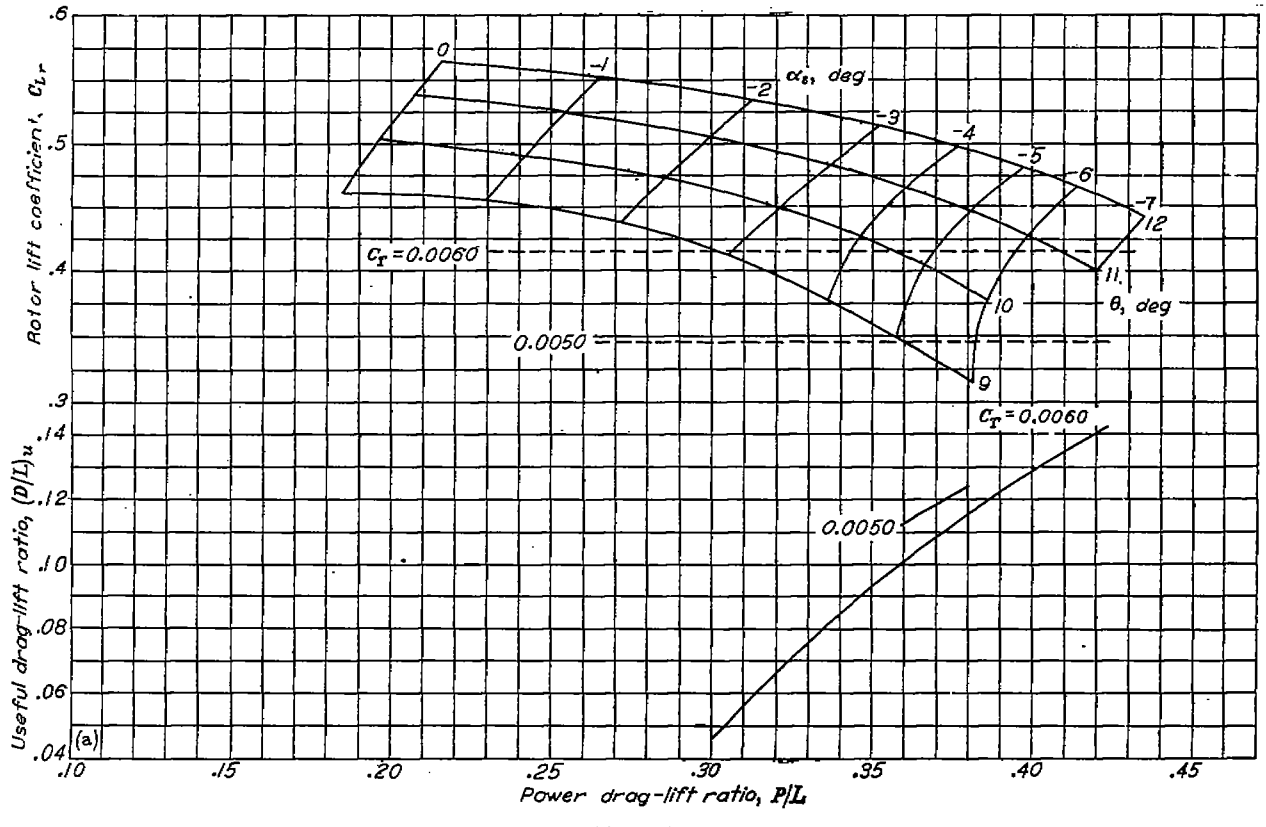

(a) $\mu=0.17$.

FIGURE 12.—Aerodynamic characteristics of the production rotor.

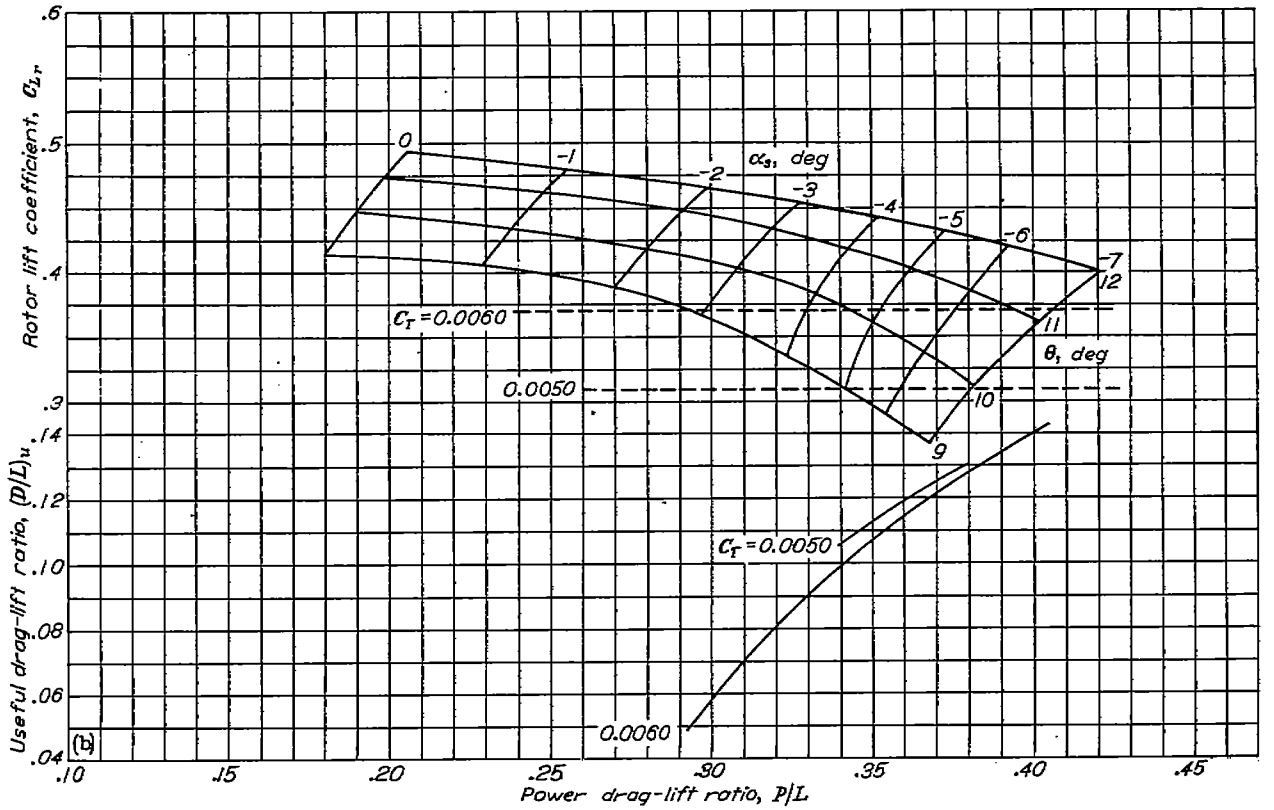

(b) μ=0.18.

FIGURE 12.—Continued.

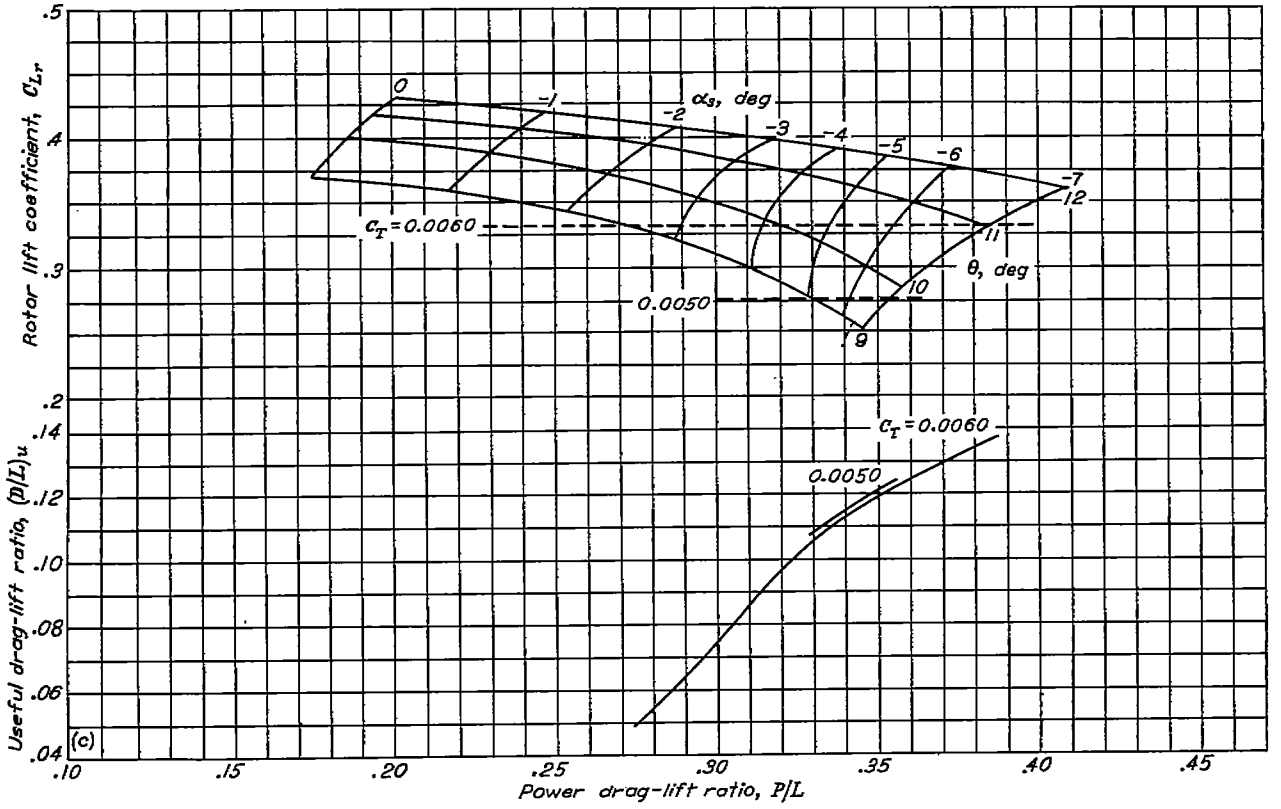

(c) μ=0.19.

FIGURE 12.—Continued.

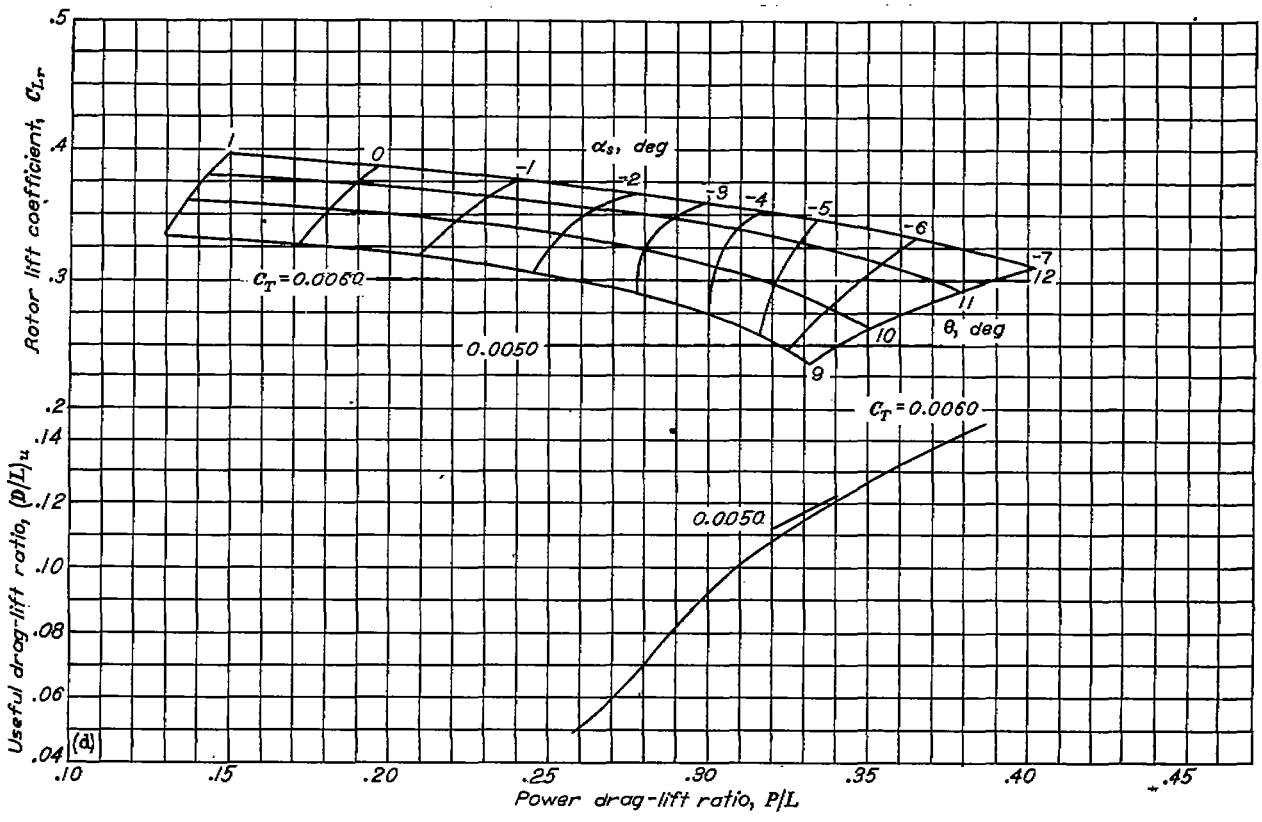

(d) μ=0.20.

FIGURE 12—Continued.

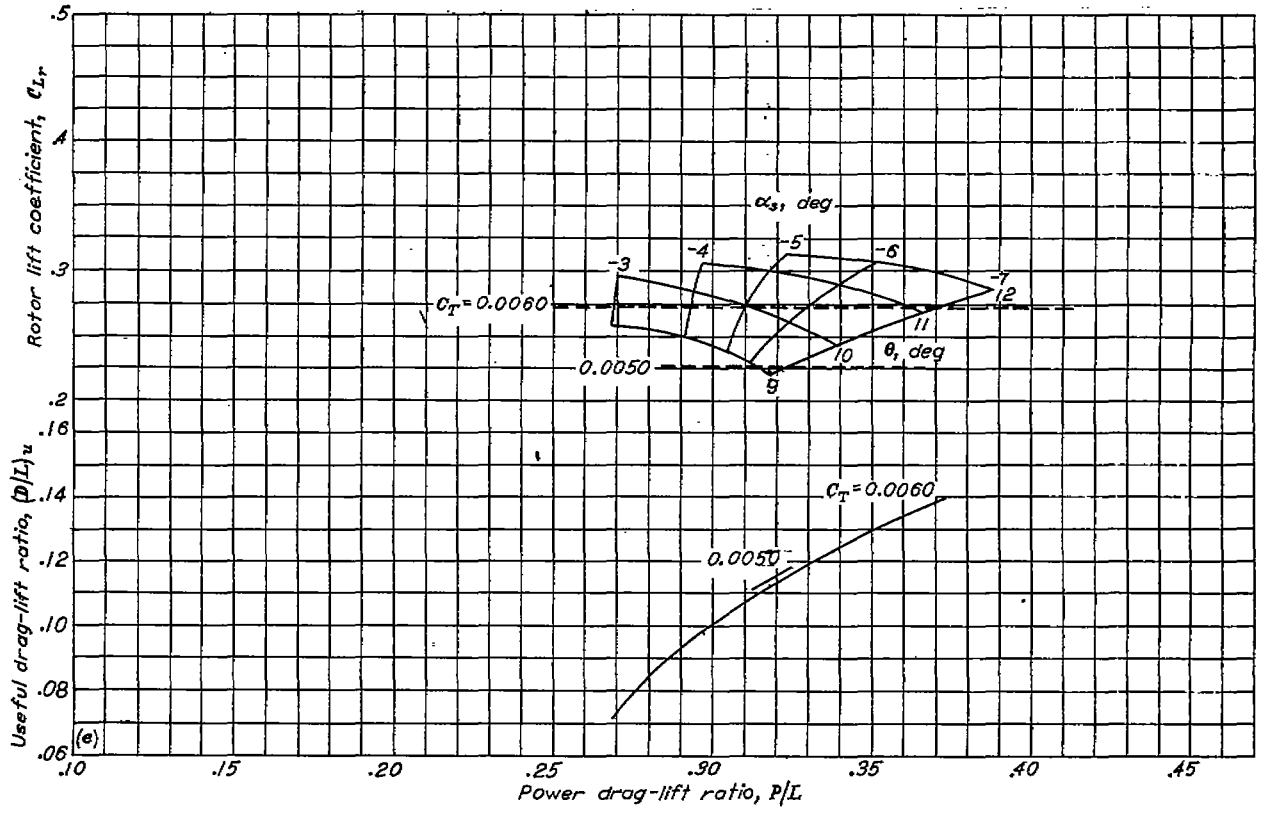

(e) μ=0.21.

FIGURE 12.—Continued.

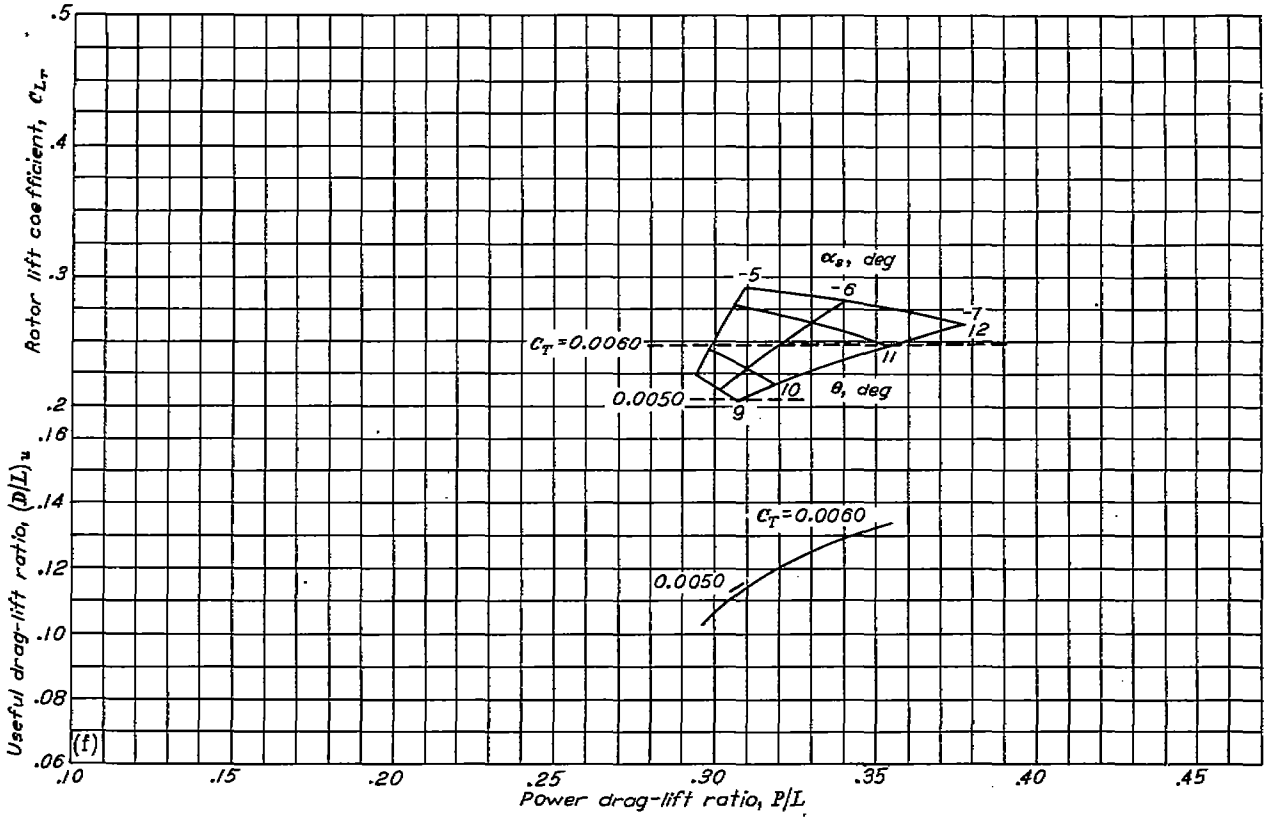

(f) μ=0.22.

FIGURE 12.—Concluded.

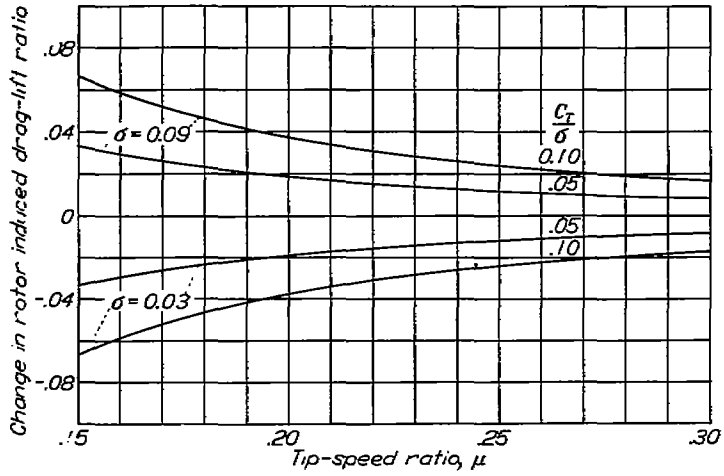

FIGURE 13.—Correction to be applied to power drag-lift ratios obtained from charts for rotors having solidities of 0.03 and 0.09.

The large performance gains that can be obtained from rotor blades which have less profile drag because of an improved surface condition are clearly shown by the results of the tunnel tests. Over the range of airspeeds for which the data for the two rotors overlap, at a thrust coefficient of 0.0060, the smooth blades require an average of 14 horsepower less than the production blades. This reduction represents an average power saving of approximately 13 percent. These results indicate that the absence or presence of a satisfactory blade surface condition could mean the difference between unacceptable and acceptable forward-flight performance. The static-thrust results of reference 1

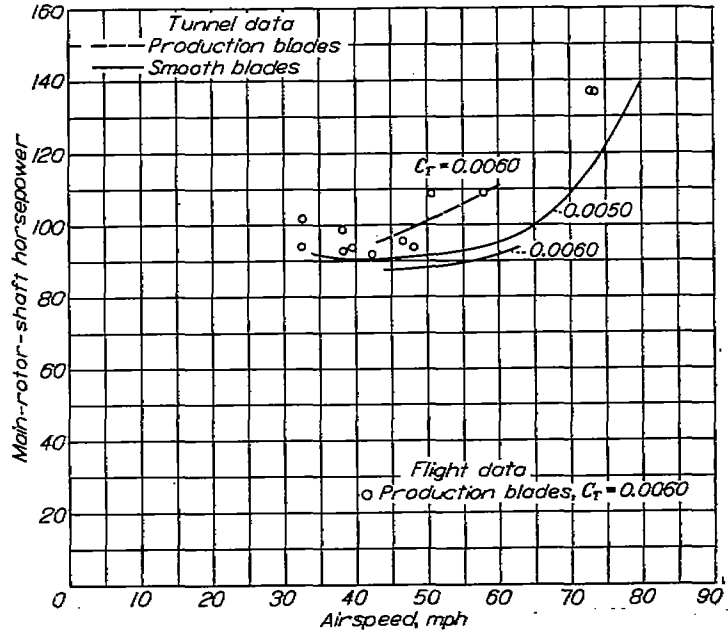

FIGURE 14.—Power required in trimmed flight over a range of airspeeds by the smooth rotor and the production rotor, and a comparison of the tunnel results with flight data for the production rotor. Gross weight, 2560 pounds; $\frac{\rho}{\rho_0}$=0.924.

and the results shown in figure 9, as well as the theoretical calculations presented in reference 5, proved that very substantial power savings can be obtained in all phases of powered flight by using rotor blades having a smooth and accurately contoured surface that will not deform during flight.

The data for the smooth blades also indicate that additional power savings are available at a given airspeed by flying at lower rotor speeds which correspond to higher thrust coefficients. An average of 3.5 percent less horsepower is required for flight at a rotor speed of 200 rpm (C_T=0.0060) than at 219 rpm (C_T=0.0050). This saving may be attributed to the larger profile lift-drag ratios resulting from the higher blade section angles of attack present at lower rotor speeds. However, the extent to which the rotor speed can be reduced will be limited by blade stalling.

Figure 14 shows that the limited amount of data obtained with the production blades is in good agreement with results of flight tests made with a similar rotor.

In order to determine how closely the results could have been predicted by theory, a comparison was made between the full-scale-tunnel data and calculations based on the charts of reference 3 for the helicopter flying with the smooth blades in level flight. Figure 15 presents a comparison of the forward-flight performance of the helicopter equipped with the smooth blades as determined from the tunnel results and as calculated by the charts of reference 3. The figure gives the horsepower required for level flight at thrust coefficients of 0.0050 and 0.0060 and shows fair agreement between the two methods.

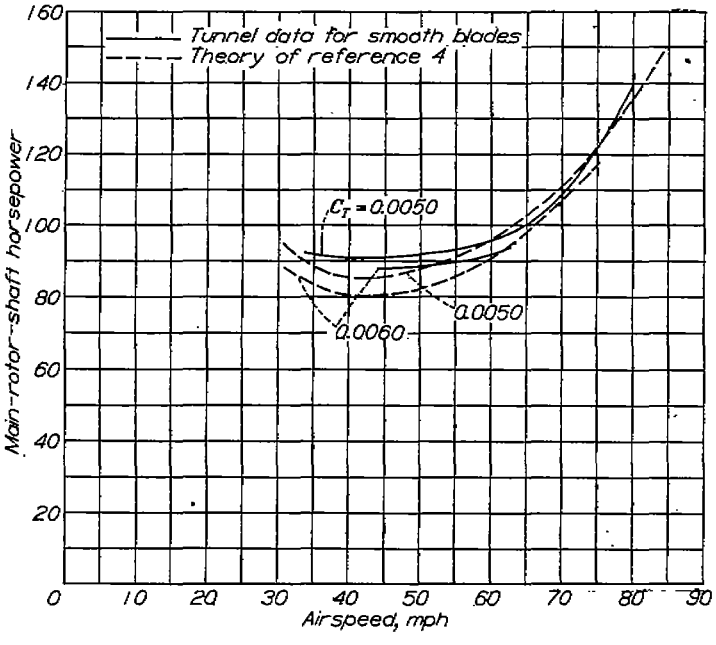

FIGURE 15.—A comparison of the experimentally determined forward-flight performance of the helicopter with that determined from theory. Gross weight, 2560 pounds; $\frac{\rho}{\rho_0}$=0.924.

CONCLUSIONS

The results of the investigation of a typical single-rotor helicopter in simulated forward-flight conditions in the Langley full-scale tunnel are as follows:

1. A smoother, more accurately and permanently contoured rotor than the production rotor will permit the helicopter to fly at a substantial reduction in the power required at any thrust coefficient because of lower profile-drag losses. At a thrust coefficient of 0.0060 the smooth-surface rotor required an average of 13 percent less power for flight over the range of airspeeds from 44 to 60 miles per hour than did the production rotor. The presence or lack of a smooth rotor-blade surface condition can constitute the difference between acceptable or unacceptable helicopter performance.

2. Additional but smaller power savings were realized in operation at higher thrust coefficients. An average of 3.5 percent less horsepower was required in flight at a rotor speed of 200 rpm (thrust coefficient, 0.0060) than at 219 rpm (thrust coefficient, 0.0050).

3. The results of the wind-tunnel investigation are shown to be in fair agreement with results of flight tests and with the predictions made from the existing theory.

LANGLEY MEMORIAL AERONAUTICAL LABORATORY,
NATIONAL ADVISORY COMMITTEE FOR AERONAUTICS,
LANGLEY FIELD, VA., *February 18, 1947.*

REFERENCES

1. Dingeldein, Richard C., and Schaefer, Raymond F.: Static-Thrust Tests of Six Rotor-Blade Designs on a Helicopter in the Langley Full-Scale Tunnel. NACA ARR No. L5F25b, 1945.
2. Gustafson, F. B.: Flight Tests of the Sikorsky HNS-1 (Army YR-4B) Helicopter. I—Experimental Data on Level-Flight Performance with Original Rotor Blades. NACA MR No. L5C10, 1945.
3. Bailey, F. J., Jr., and Gustafson, F. B.: Charts for Estimation of the Characteristics of a Helicopter Rotor in Forward Flight. I—Profile Drag-Lift Ratio for Untwisted Rectangular Blades. NACA ACR No. L4HO7, 1944.
4. Bailey, F. J., Jr.: A Simplified Theoretical Method of Determining the Characteristics of a Lifting Rotor in Forward Flight. NACA Rep. No. 716, 1941.
5. Gustafson, F. B.: Effect on Helicopter Performance of Modifications in Profile-Drag Characteristics of Rotor-Blade Airfoil Sections. NACA ACR No. L4HO5, 1944.